DALTON
FULL PAPER

Continuous symmetry measures of penta-coordinate molecules: Berry and non-Berry distortions of the trigonal bipyramid †

Santiago Alvarez* and Miquel Llunell

Departament de Química Inorgànica, Departament de Química Física and Centre de Recerca en Química Teòrica (CeRQT), Universitat de Barcelona, Diagonal 647, 08028 Barcelona, Spain. E-mail: salvarez@kripto.qui.ub.es

Received 19th June 2000, Accepted 31st July 2000
First published as an Advance Article on the web 18th September 2000

The application of continuous symmetry measures to the description of the structures of penta-coordinate complexes is discussed. The characteristic values of the trigonal bipyramid symmetry measure, *S*(TBP), for molecules with square pyramidal (SP) or intermediate geometries corresponding to a Berry pseudorotation coordinate are established. The experimental data from a reference set comprising 71 structures of more than 40 homoleptic transition metal complexes (including organometallic molecules and inorganic solids) and four EPh_5 derivatives of Group 15 elements are consistent with the Berry pathway. The structures of several families of transition metal complexes are analyzed in the light of the variations of *S*(TBP) corresponding to other distortions of the ideal TBP, including bond stretch or non-Berry angular distortion modes. The families of compounds analyzed are represented by the general formulae $[OMX_4]^-$, $[NMX_4]^-$, $[Cu(bipy)_2X]^+$, $[Cu(phen)_2X]^+$, $[M(dppe)_2X]$, $[M(tripod)X]$, $[M(terpy)X_2]$, $[M(NO)L_4]$ with the $\{MNO\}^8$ electron count, vanadium-(IV) and -(V) compounds including several oxides and vanadyl complexes. The S_N2 substitution pathway in Sn compounds that had been previously shown to be well represented by the structural data of a series of compounds with, *e.g.*, a $XSnC_3O$ core are also shown to be elegantly described by the simultaneous change in their TBP and T_d continuous symmetry measures.

Avnir and co-workers have proposed that molecular symmetry should be treated as a continuous structural property.[1,2] According to these authors, rather than describing a molecular structure as having a certain symmetry or not, it is most useful to use a quantitative measure that tells us how far (or how close) that structure is from a specific symmetry. Therefore, the continuous symmetry measure (abbreviated from here on as CSM) for a molecular structure is defined as the distance to the desired shape, independent of size and orientation.

For molecules or molecular fragments that can be approximately described by a polyhedron, the coordinates of the *N* atoms are given by the vectors $\vec{Q}_k$ ($k = 1, 2, ..., N$), whereas the coordinates for the perfect polyhedron closest in size and orientation are given by the vectors $\vec{P}_k$ ($k = 1, 2, ..., N$). The *distance* of the molecular structure to the perfect polyhedron belonging to a symmetry point group *G* is then defined as[3]

$$S(G) = \frac{\sum_{k=1}^{N} |\vec{Q}_k - \vec{P}_k|^2}{\sum_{k=1}^{N} |\vec{Q}_k - \vec{Q}_0|^2} \times 100 \qquad (1)$$

where $\vec{Q}_0$ is the coordinate vector of the center of mass of the investigated structure. With such definitions, it has been shown that the boundaries for any symmetry measure are $100 \geqslant S(G) \geqslant 0$. The lower limit corresponds to structures that exactly match the shape of symmetry *G*, and increasing values result for increasingly distorted structures. A very useful property of the symmetry measures is that they allow us to compare on the same scale the proximity of different molecules to the same symmetry, or of the same molecule to different symmetries. One can also calibrate on the same scale different distortions from a particular ideal structure.

Once the concept, the methodology and a variety of interesting applications[1] of the continuous symmetry measure have been established, we wish to explore the real meaning that can be attached to the numerical values obtained, and their applicability to the description and discussion of the stereochemistry of coordination polyhedra. In particular, we are interested in the possible use of CSM as a tool for rationalizing large amounts of structural data and associated chemical information. In this paper we focus on the penta-coordinate molecules, for which there is a wide range of structural variation. The two ideal structures for a penta-coordinate complex are the trigonal bipyramid (TBP) of D_{3h} symmetry, and the square pyramid (SP) of C_{4v} symmetry, but in many cases intermediate structures can be found. The same molecule may even appear in different coordination environments in different crystal structures or in different crystallographic positions of the same crystal structure. The trigonal bipyramid is not uniquely defined, since an AB_5 molecule may present different axial and equatorial distances without losing the ideal D_{3h} symmetry. In a recent study of the ideal coordination polyhedra[4] it was shown that a reasonable choice from the chemical point of view is to take a trigonal bipyramid with all A–B distances the same as a reference polyhedron. Hence, throughout this paper we will use the symmetry measure *S*(TBP) as the distance of a structure (in the sense of eqn. (1)) to an equidistance trigonal bipyramid.

A simple and useful angular parameter commonly used for penta-coordinate complexes is that proposed by Addison *et al.*[5] defined as

$$\tau = (\alpha - \beta)/60 \qquad (2)$$

To make the definition of τ unambiguous and amenable to automatic computation from crystal structure data, we adopt

† Electronic supplementary information (ESI) available: tables of REFCODES, relevant structural information and calculated symmetry measures. See http://www.rsc.org/suppdata/dt/b0/b004878j/

 DOI: 10.1039/b004878j

the convention that α and β are the two largest L–M–L bond angles, with $\alpha \geqslant \beta$. In a perfect TBP, $\alpha = 180°$ and $\beta = 120°$, resulting in $\tau = 1$. On the other hand, an ideal square pyramid has $\alpha = \beta$, and its angular parameter is $\tau = 0$. Therefore, any structure intermediate between SP and TBP (*i.e.*, along the Berry distortion coordinate) must have an angular parameter in the range $0 \leqslant \tau \leqslant 1$. Some differences between the angular parameter τ and *S*(TBP) can be envisaged. The former does not take into account inequivalences in bond distances, neither is it expected to correctly reflect angular distortions other than the Berry pseudorotation. Conversely, the symmetry measure *S*(TBP) tells us in principle how distant a structure is from a perfect TBP but not in which way it is distorted.

The aim of this paper is to present a comprehensive exploration of the different distortions of the trigonal bipyramid in terms of the corresponding symmetry measures. With such exploration we expect to learn about the meaning of the numerical values of the continuous symmetry measure *S*(TBP), but also to provide some guidelines for the systematics of structural analysis of penta-coordinate atoms in organometallic, coordination and solid state compounds.

We will first analyze the effect of different distortions of an ideal ML_5 group on its symmetry measure, classifying them according to the symmetry-adapted normal modes. The model expectations will be compared to the symmetry measures of homoleptic complexes calculated from their crystal structural data. We use as a benchmark data set a collection of structures comprising homoleptic transition metal complexes ML_5 (Table 1), penta-coordinate MX_5 fragments in several inorganic solids (Table 2) and the family of pentaphenyl derivatives of the Group 15 elements, EPh_5 (Table 3). Three groups of distortions will be separately discussed: (i) those involving only changes in bond lengths, (ii) the angular Berry distortion leading to the square pyramid and (iii) other angular non-Berry distortions.

Other sections of this paper will be devoted to showing the specific behavior of important families of penta-coordinate compounds. First, we will show how the combined use of the tetrahedral and TBP symmetry measures provide an elegant description of the S_N2 pathway evidenced by the crystal structures of the families of $SnR_3(OR')$, SnR_3X and $SnR_3X(OR')$ compounds. Then we will discuss the effect of bidentate, tridentate or tripod ligands on the distortion pathways, the expression in terms of continuous symmetry measures of the edge-capped tetrahedral geometry of penta-coordination, and the specific application of this methodology to vanadium oxides and vanadyl complexes, as well as to metal nitrosyl complexes.

Bond length distortion modes of a trigonal bipyramid

Throughout this paper we will label the distortions of the trigonal bipyramid making reference to the related normal vibrational coordinates,[72] separately considering the stretching and bending modes. In practice, one can find structures that correspond to the simultaneous application of two or more such modes, but their effect on the symmetry measure is easier to understand if we apply them first to ideal molecules independently. In later sections, we will be able to identify such distortion modes in the experimental structures.

Let us first analyze those distortions of the trigonal bipyramid that consist of stretching one or more M–L bonds simultaneously, while keeping the bond angles untouched and the rest of the bond lengths fixed at an arbitrary distance of 2.25 Å, as schematically represented in Chart 1. The symmetry measures obtained for such distortions are presented in Fig. 1a as a function of the ratio between the two different bond distances. For a particular distortion mode, the actual value of *S*(TBP) depends not only on the ratio between long and short distances, but also on the bond distances themselves. However, the differences in *S*(TBP) are not significant for distance ratios

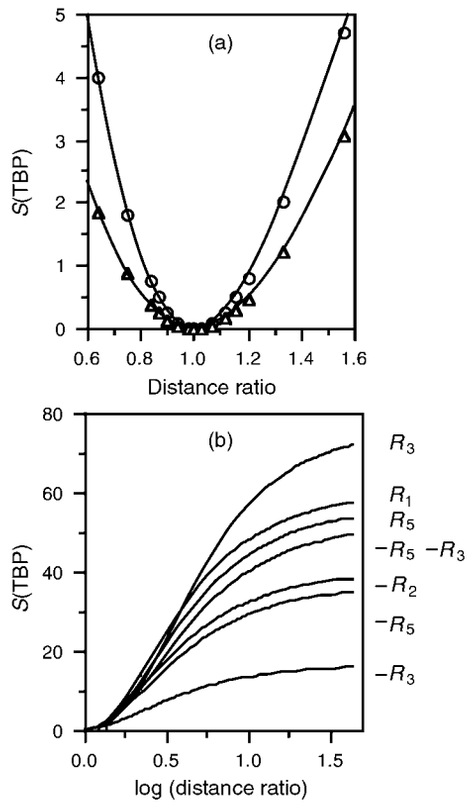

Fig. 1 (a) TBP symmetry measure of an ML_5 molecule as a function of the bond stretching distortions R_1 (circles) and R_3 (triangles) represented in Chart 1. Distance ratios of less than one for R_1 are equivalent to axial bond stretching R_2. The values obtained for R_5 (not shown) are intermediate between the two curves presented here. (b) TBP symmetry measure for an ML_5 molecule upon different bond stretching distortion modes (see Chart 1), plotted as a function of the log of the distance ratio.

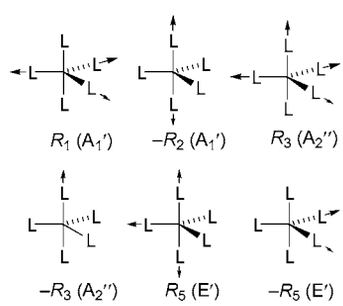

Chart 1

of up to 1.5:1. It is noteworthy that small distortions (*e.g.*, of less than 0.1 Å) produce only minute variations in the *S*(TBP) values. For comparison, the symmetry decrease produced by bending the L_{ax}–M–L_{ax} bond angle to 178° is equivalent to that induced by a distortion of bond distances as large as 0.1 Å, *i.e.*, these two structures are *isosymmetric*. For distortions at distance ratios of less than 1.2:1, the *S*(TBP) values are in all cases at most 0.8.

For very large M–L separations, the different bond stretch distortion modes give a limiting *S*(TBP) value, as reported earlier for the case of axial compression or elongation.[3] What is interesting to stress is that the limiting values for the distortion modes applied here can be grouped by the number of bonds stretched in each case. Hence, the limit for *S*(TBP) is ≈70 when four bonds are stretched, between 50 and 60 for three bonds, 35–40 for two bonds, and about 15 when only one bond is elongated.

Table 1 Trigonal bipyramidal continuous symmetry measure *S*(TBP) and angular parameter τ for homoleptic ML_5 transition metal complexes of d^n electron configuration. The pyramidality angle π (see Chart 2, **a**) is also given for complexes with nearly perfect square pyramid geometry, *S*(TBP) ≤ 0.1

Compound	*n*	τ	*S*(TBP)	π	REFCODE	Ref.
$[CdCl_5]^{3-}$	10	1.000	0.005			6
$[HgCl_5]^{3-}$	10	0.518	3.375		FAHVEP	7
$[HgCl_5]^{3-}$	10	1.000	0.052			8
$[CuCl_5]^{3-}$	9	0.003	5.693	97.4	AEPIPC	9
$[CuCl_5]^{3-}$	9	1.000	0.036			10
$[CuCl_5]^{3-}$	9	1.000	0.035			11
$[CuBr_5]^{3-}$	9	1.000	0.004			12
$[CuBr_5]^{3-}$	9	0.171	3.978		GADSEJ	13
$[CuBr_5]^{3-}$	9	0.067	5.137		GECFAV	14
$[CuBr_5]^{3-}$	9	0.026	5.942	94.1	GECFAV	14
$[Cu(NH_3)_5]^{2+}$	9	0.025	5.395	97.6		15
$[Cu(NCS)_5]^{3-}$	9	0.000	5.589	98.4	JONZIV	16
$[Cu(Im)_5]^{2+}$	9	0.924	5.674	95.9	CUTBEY	17
$[Cu(O{=}Im)_5]^{2+}$ [a]	9	0.015	5.984	93.4	IMZCUP	18
$[Mn(CO)_5]^-$	8	0.940	0.118		FUDKAQ	19
$[Mn(CO)_5]^-$	8	0.946	0.021		VAGFEO	20
$[Mn(CO)_5]^-$	8	0.937	0.075		JOLWEM	21
$[Mn(CO)_5]^-$	8	0.914	0.116		TADPET	22
$[Mn(CO)_5]^-$	8	0.887	0.089		PNIMNC10	23
$[Mn(CO)_5]^-$	8	0.920	0.067		PNIMNC10	23
$[Mn(CO)_5]^-$	8	0.904	0.186		YUGWOM	24
$[Mn(CO)_5]^-$	8	0.881	0.175		YUGWOM	24
$[Mn(CO)_5]^-$	8	0.795	0.267		HCPDNB10	25
$[Mn(CO)_5]^-$	8	0.000	5.475	102.6	TOJGII	26
$[Fe(CO)_5]$	8	0.964	0.018		FOJBOV03	27
$[Mn(CNC_6H_3Me_2\text{-}2,6)_5]^-$	8	0.836	0.622		RAGHOW	28
$[Fe(CN^tBu)_5]$	8	0.322	2.636		PTBICF10	29
$[Fe(CN^tBu)_5]$	8	0.515	1.364		PTBICF10	29
$[CoH_5]^{4-}$	8	0.000	5.761	97.6		30
$[Ni(OAsMe_3)_5]^{2+}$	8	0.187	3.877		MASONI	31
$[Ni(P\{OEt\}_3)_5]^{2+}$	8	0.912	0.069		OXPHAD10	32
$[Ni(CN)_5]^{3-}$	8	0.008	5.446	99.2	CRTNCN01	33
$[Ni(CN)_5]^{3-}$	8	0.007	5.463	100.2	EDCRCN	34
$[Ni(CN)_5]^{3-}$	8	0.288	3.296		VUTRAD	35
$[Ni(CN)_5]^{3-}$	8	0.528	1.403		EDCRCN	34
$[Pt(GeCl_3)_5]^{3-}$	8	0.570	1.193		TMAGEP	36
$[Pt(SnCl_3)_5]^{3-}$	8	1.000	0.002		BENLUB	37
$[Co(ONC_5H_3Me\text{-}o)_5]^{2+}$	7	0.727	0.764		PICOCO01	38
$[Co(CNPh)_5]^{2+}$	7	0.033	5.874	95.1	PICNCO	39
$[Co(CNPh)_5]^{2+}$	7	0.000	5.501	101.8	PICYCO	40
$[Co(CN)_5]^{3-}$	7	0.000	5.765	97.7	EIPCYC10	41
$[Co(CN)_5]^{3-}$	7	0.000	6.166	95.0	ZIHTIT	42
$[Co(CN)_5]^{3-}$	7	0.085	4.795		ZIHTEP	42
$[Co(CNMe)_5]^{2+}$	7	0.836	0.129		MINCOP	43
$[Co(CNC_6H_4Me\text{-}p)_5]^{2+}$	7	0.896	0.406		BAMNIM	44
$[Rh(C_6F_5)_5]^{2-}$	7	0.039	6.374	96.0	SAHWAZ	45
$[FeCl_5]^{2-}$	5	0.960	0.058		YOZRAG	46
$[FeCl_5]^{2-}$	5	1.005	0.277		HITVOV	47
$[MnCl_5]^{2-}$	4	0.240	3.321		PYTZCM	48
$[VCl_5]^-$	1	0.924	0.077		DOTPAD	49
$[TiMe_5]^-$	0	0.405	2.038			50
$[TiMe_5]^-$	0	0.740	0.474			50
$[Nb(OC_6H_3\text{-}2,6\text{-}Me_2)_5]$	0	0.841	0.202		KARVII	51
$[Ta(CH_2C_6H_4Me\text{-}p)_5]$	0	0.018	5.520	111.0	HEDKUW	52
$[Ta(O^iPr)_5]^-$	0	0.774	0.464		ZIMXOI	53
$[Ta(SC_6HMe_4)_5]$	0	0.454	2.297		YICPUV	54
$[La(OC_6H_4{}^iPr\text{-}o)_5]^{2-}$	0	0.839	0.360		TOCXUE	55

[a] O=Im stands for imidazolidinone.

The analysis of a variety of experimental structures has shown us (see subsequent sections) that angular distortions are in most cases responsible for the large variations in the TBP symmetry measure, whereas differences in bond distances are responsible only for a smaller part of the observed dispersion in the *S*(TBP) values. However, there are some interesting examples in which a loss of TBP-ness is clearly associated with bond stretching distortions. A clear case of an asymmetric expansion of the TBP in the equatorial direction is provided by the diethylenetriammonium salt of the $[HgCl_5]^{3-}$ anion.[7] The angular parameter for this anion ($\tau = 0.52$) suggests a structure intermediate between TBP and SP, but its symmetry measure (3.37) seems too large compared to, *e.g.*, the two crystallographically independent anions $[Ni(CN)_5]^{3-}$ in the salt[34] with $[Cr(en)_3]^{3+}$ as counter ion, with similar values of τ, but much smaller symmetry measures (1.40). It is thus clear that the strong loss of TBP symmetry in $[HgCl_5]^{3-}$ is not attributable to angular distortions. A look at the structure shows the existence of remarkable differences between the axial (2.3 Å) and equatorial (3.1 Å) Hg–Cl bond distances. We can conclude that the large value of *S*(TBP) is consistent with a description of this anion as a two-coordinate linear $[HgCl_2]$ complex with three "contacts" to chloride ions.

The opposite distortion appears in the active site of the blue copper protein Azurin from *Alcaligenes denitrificans*,[73,74] with three short bonds (≈2.1 Å) from two histidine and one cysteine

Table 2 Trigonal bipyramidal continuous symmetry measure S(TBP) and angular parameter τ for transition metal homoleptic MX_5 fragments of d^n electron configuration in extended structures. The pyramidality angle π (see Chart 2, **a**) is also given for complexes with nearly perfect square pyramid geometry, $S(TBP) \leqslant 0.1$

M	X	Compound	n	τ	S(TBP)	π	Ref.
Cu	O	$CuAlInO_4$	9	1.025	0.307		56
Cu	O	$CuGaInO_4$	9	1.028	0.360		57
Cu	O	$Cu_2(AsO_4)OH$	9	0.738	1.231		58
Cu	O	$YBa_2Cu_3O_7$	9	0.014	5.421	97.9	59
Cu	O	$YBa_2Cu_3O_6$	9	0.000	5.761	97.6	60
Cu	O	$Tl_2Ba_2Ca_2Cu_3O_{10}$	9	0.000	6.102		61
Ni	Ge	$LaNiGe_2$	8	0.011	6.652	118.1	62
Ni	Ge	$SmNi_3Ge_3$	8	0.000	7.806	121.8	63
Mn	O	$Ca_4Mn_2O_7$	6	0.000	7.474	90.0	64
Mn	O	$Ca_2Mn_2O_5$	6	0.171	4.497		64
Re	O	$Ba_5(ReO_5)_3Cl$	0	0.000	5.587	109.2	65

Table 3 Trigonal bipyramidal continuous symmetry measure S(TBP) and angular parameter τ for EPh_5 compounds (E is a Group 15 element)

Compound	τ	S(TBP)	REFCODE	Ref.
PPh_5	0.937	0.238	PHENYP	66
$AsPh_5$	0.977	0.194	PENPAS	67
$SbPh_5$	0.246	3.336	PHENSB01	68
$SbPh_5$	0.951	0.105	PPHSBC	69
$BiPh_5$	0.252	3.542	HAKVOE	70
$BiPh_5$	0.221	3.552	SAKZUZ	71

group in a trigonal planar environment, complemented by two long contacts (≈3.1 Å) to a glycinate and a methionine, resulting in a severely elongated trigonal bipyramid, with a TBP symmetry measure of 7.29. The small value of the angular parameter ($\tau = 0.17$) would suggest a structure close to a square pyramid, but we will see in the next section that square pyramids with all bond distances equal are expected to give S values smaller than 6.5, and a larger S value is a clear indication of a severe bond length distortion in addition to the angular deformation towards SP, in keeping with the description of such active site as a three-coordinate center with two contacts at long distances.

Angular distortions: the Berry pseudorotation pathway and the square pyramid

The symmetry properties of different angular distortion modes[72] for penta-coordinate groups are summarized in Table 4. Throughout this paper we will use simplified versions of the normal modes schematically represented by the internal coordinates R_i (Chart 2 and Table 4). The families of compounds discussed below for which the corresponding distortions have been identified are also indicated in Table 4.

The Berry pseudorotation pathway[75] is actually a combination of the equatorial R_6 and axial R_7 bending modes of E' symmetry represented in **a**. This mode exchanges the equatorial and axial ligands of a trigonal bipyramid through a square pyramidal intermediate. Muetterties[76] and Bürgi[77] have shown that such rearrangement can be described by a sequence of crystal structures. According to Muetterties, the proximity of a given molecule to ideal TBP or SP polyhedra can be established by the analysis of the set of torsion angles between the edges of the polyhedra. Kepert,[78] on the other hand, used two polar coordinates (assuming all bond distances equal) within C_{2v} symmetry to define the Berry pathway. These two approaches require the use of more than one structural parameter to classify the position of a molecule along the Berry pathway. In contrast, both the angular parameter τ and the CSM allow us to describe the Berry distortion with a single parameter, and we explore here their main characteristics and advantages.

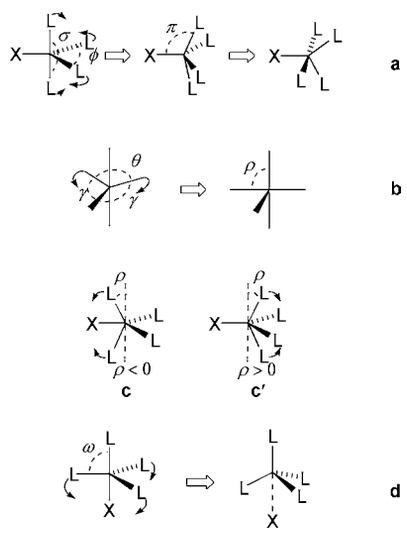

Chart 2

In our definition of the C_{2v} Berry pseudorotation coordinate **a**, the bond angles σ and ϕ vary in a concerted way from a TBP ($\sigma = 180°$, $\phi = 120°$) to an SP ($\sigma = \phi = 105°$) to a pseudorotated TBP ($\sigma = 120°$, $\phi = 180°$). In Fig. 2a we show how these two parameters, τ and S(TBP), evolve along that path. While τ has a linear dependence on the reaction coordinate, the symmetry measure changes smoothly for small angular deviations from TBP and increases sharply when approaching the square pyramid, reaching a maximum value of $S(TBP) = 5.4$. A striking result, due to the different dependence of the two parameters on σ, is that a molecule with $\tau = 0.5$ is halfway in the TBP to SP path in terms of angular deformation, but seems to be still much closer to the TBP than to the SP in terms of symmetry, $S(TBP) = 1.36$. The relationship between the two parameters can be seen in Fig. 2b (lower line) for an ideal ML_5 molecule with five identical bond distances. Such a plot gives a lower limit of the symmetry measure at a given value of τ. As an example of how bond distance inequality affects the symmetry measure, we show also the S(TBP) values for the case in which the M–X/M–L bond distance ratio is 0.7 : 1 (Fig. 2b, upper line). Clearly, the ideal equidistance bipyramid, $S(TBP) = 0.0$, cannot be attained with unequal bond distances, and the symmetry measure is higher than for the equidistance molecule for any value of the angular parameter τ.

The experimental structural data for our reference set of structures (Tables 1–3) are shown in Fig. 2b for comparison with the ideal Berry pathway (circles and squares for transition metals, Tables 1 and 2; triangles for the EPh_5 compounds, Table 3). Such data are nicely distributed along the Berry coordinate, irrespective of the variety of central atoms and ligands comprised in these three families. The most significant deviations appear for those structures with $\tau \approx 0$, for which S(TBP)

Table 4 Angular distortion modes (D_{3h} point group) for a trigonal bipyramidal AX_5 fragment[a]

Coordinate	Name	Chart	Parameter	G	G'	Examples
$R_6 + R_7$ (E')	Berry	**2a**	σ, ϕ	C_{2v}	C_{4v}	ML_5, MX_5, EPh_5, MOX_4, MNX_4
R_6 (E')	Y	**2b**	θ, γ	C_{2v}	C_{2v}	$[M(chel)_2X]$, [Cu(terpy)X]
$-R_6$ (E')	T	**4e**,**f**	θ, γ	C_{2v}	C_{4v}	$[M(chel)_2X]$, [Cu(terpy)X]
R_7 (E')	Reverse Berry	**2c**	ρ	C_{2v}	C_{2v}	$[MCp_2L_2X]$
R_4 (A''_2)	Umbrella	**2d**	ω	C_{3v}	T_d	[M(tripod)L], S_N2 at Sn

[a] $[M(chel)_2X]$ are complexes of the families $[Cu(bipy)_2X]$, $[Cu(phen)_2X]$ or $[M(dppe)_2X]$, where M is any transition metal and X is any monodentate ligand. G is the symmetry subgroup to which the molecule belongs after distortion, and G' is a symmetry point group that can eventually be reached along the distortion coordinate.

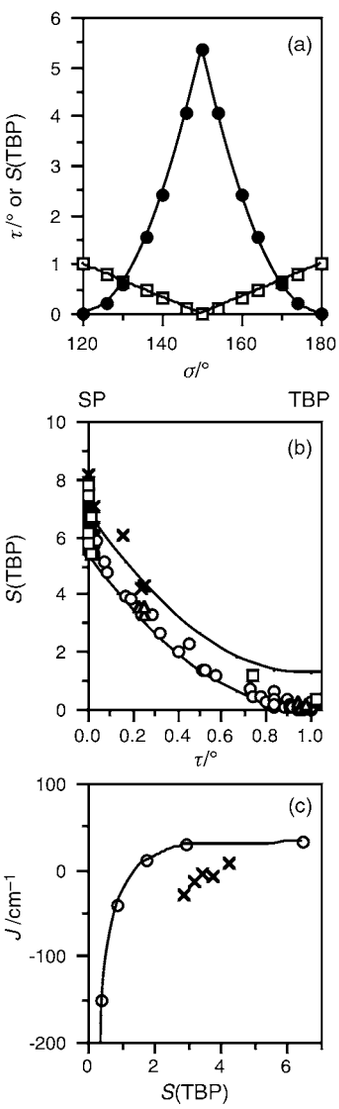

Fig. 2 (a) Evolution of the angular parameter τ (eqn. (2), squares) and of the TBP symmetry measure (circles) along the Berry pseudorotation pathway. (b) Relationship between the TBP symmetry measure and the angular parameter τ for an ML_5 molecule (continuous lines) with all bond distances equal (lower line) and for XML_4 groups with an M–X/M–L distance ratio of 0.7:1 (upper line). Also plotted are the experimental structural data for homoleptic transition metal complexes (circles), MX_5 fragments in extended structures (squares), EPh_5 compounds of Group 15 elements (triangles), and $[OMX_4]^-$ complexes (crosses; M = Cr, Mo, W; X = Cl, Br, I). (c) Exchange coupling constant for binuclear Cu(II) complexes with two end-to-end azido bridges as a function of the TBP symmetry measure. Calculated values are represented by circles[81] and experimental ones by crosses.

adopts values between 5 and 6.5. In contrast, all the $[OMX_4]^-$ anions (M = Cr, Mo, W; X = Cl, Br, I; crosses in Fig. 2b) present perfect or slightly distorted square pyramidal structures. Again, some dispersion of the S(TBP) values appear for the perfect SP oxoanions (6.6–8.2), a problem that will be addressed later in this paper.

Several authors have noted previously that the trigonal bipyramid and the square pyramid are quite close in energy in many cases, as indicated by both molecular orbital arguments[79] and electrostatic ligand repulsion calculations.[78] Experimentally, for instance, the $[Mn(CO)_5]^-$ and $[CuCl_5]^{3-}$ anions, or the CuO_5 group in several salts, can be found in either form as indicated by both the angular parameter τ and the TBP symmetry measure (Table 1). Interestingly, the molecular structures collected for such fragments do not show intermediate geometries. The $[Ni(CN)_5]^{3-}$ anion, in contrast, appears as a square pyramid, distorted or not, but not as a trigonal bipyramid. The opposite happens with the d^{10} complexes $[MCl_5]^{3-}$ (M = Cd, Hg), that are trigonal bipyramids, regular or distorted, but do not seem to distort all the way to the square pyramid. In contrast, the Zn analog[80] is far from a TBP as reflected by S(TBP) = 4.83, even if its angular parameter (τ = 0.76) is indicative of a slightly distorted TBP. This is because one of the axial Zn–Cl distances is very long, a distortion that will be discussed in more detail below.

An example of how physical properties can be described in terms of local symmetry can be found in our recent study of the magnetic exchange interaction between Cu(II) ions bridged by two azido ligands.[81] We calculated the exchange coupling constant for a model of these $[Cu_2(\mu\text{-}N_3)_2L_6]$ complexes with $L = NH_3$, and found that it becomes negative (indicating antiferromagnetic coupling) as the geometry around the two copper atoms approach the TBP, as illustrated nicely through the dependence of J on S(TBP) (Fig. 2c, circles). A similar dependence, with some quantitative differences, can be found for the experimental data (Fig. 2c, crosses).

We have seen above that a variety of S(TBP) values are found for molecules which can be defined as square pyramids according to the angular parameter ($\tau \approx 0$). This result has to do with the fact that square pyramids differ from each other in their degree of pyramidality measured by the L_{ax}–M–L_{eq} bond angle (π in **a**). The angular parameter τ recognizes all square pyramids as such ($\tau = 0$), regardless of their degree of pyramidality π. In contrast, the value of the symmetry measure provides some information on both the square pyramidal nature of the structure, its pyramidality angle, and differences in bond lengths. To illustrate this, we present in Fig. 3 the symmetry measure obtained for an ideal square pyramidal molecule with all bond distances equal (lower line), as a function of the pyramidality angle. It can be seen that the maximum TBP-ness of an equidistance square pyramid corresponds to $\pi = 105.8°$, for which S(TBP) = 5.37. The symmetry measures for the experimental structures of square pyramidal transition metal fragments (*i.e.*, those with $\tau \approx 0$) closely follow the theoretical expectations, thus accounting for the dispersion found in the $S(\tau)$ curve discussed above (Fig. 2a). Most of the structures in our reference set (Table 1) correspond to pyramidality angles in the range $93 < \pi < 105°$, although there are a few exceptions with larger bond angles: the organometallic complex $[Ta(CH_2C_6H_4Me\text{-}p)_5]$[52] ($\pi = 111.0°$) and the $NiGe_5$ fragment in the solid state compounds $LaNiGe_2$ and $SmNi_3Ge_3$ ($\pi = 118.1$[62]

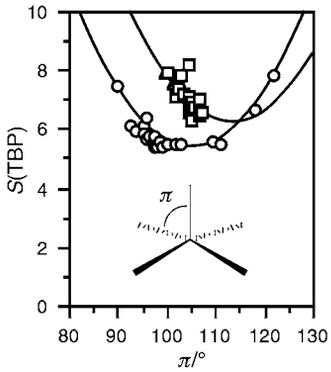

Fig. 3 TBP symmetry measure for a C_{4v} square pyramid ML_5 as a function of the pyramidality angle π (**a**), as calculated for a model compound with all M–L distances equal (lower line) and with a distance ratio $t = 0.7:1$ (upper line). Also plotted are the experimental structural data corresponding to homoleptic $[ML_5]$ complexes or MX_5 fragments in extended solids (white circles, data in Tables 1 and 2) as well as to mixed ligand $[OMX_4]$ (squares) and $[NMX_4]$ (triangles) complexes (distance ratios $0.68 < t < 0.72$) with nearly perfect square pyramidal structure ($\tau \approx 0$).

and 121.8°,[63] respectively). Even if the set of homoleptic penta-coordinate structures analyzed here is not comprehensive, the latter example seems to be a good candidate for the world record of pyramidality.

A common structural feature of mixed ligand complexes of formulae $[OMX_4]$ or $[NMX_4]$, where M is a transition metal and X is a halide, is the presence of a very short M–O or M–N bond distance compared to the M–X ones. Hence, it is of interest to analyze how the inequality in bond distances affects the symmetry measure of the square pyramids. Assuming an ABX_4 square pyramid with C_{4v} symmetry, and defining the axial to basal bond distance ratio as t = A–B/A–X we have studied the dependence of S(TBP) on the pyramidality angle π for different t values. The ideal parabolic behavior of the equidistances pyramid represented in Fig. 3 is retained when the distance ratio is varied, but the position of the parabola changes. In summary, the pyramidality angle with the maximum TBP symmetry depends linearly on the distance ratio (Fig. 4a), whereas the minimum S(TBP) value of a square pyramid shows a parabolic dependence on t (Fig. 4b). According to those results, the SP closest to a trigonal bipyramid is one with $t = 1.05$ and $\pi = 104.9°$, for which S(TBP) is 5.35.

In order to compare these results with experimental data, we represent S(TBP) as a function of π for a distance ratio $t = 0.7:1$, typically found in the $[OMX_4]^-$ (M = Cr, Mo, W; X = Cl, Br, I) anions (Fig. 3, upper line). The symmetry measures for the experimental structures of $[OMX_4]^-$ and $[NMX_4]^-$ (M = Mo, Tc, Re, Ru, Os) with $\tau \approx 0$ nicely illustrate how the unequal bond distances results in higher S(TBP) values for perfect square pyramids of the same pyramidality angle.

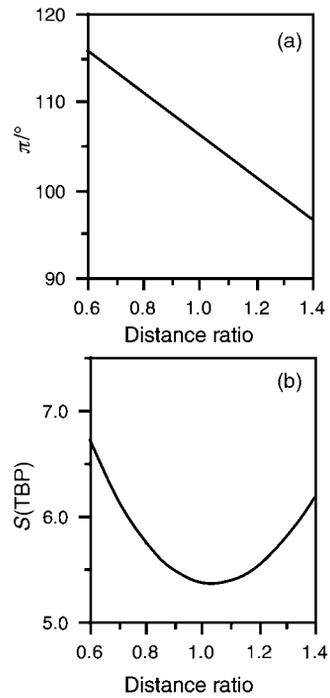

Fig. 4 (a) Pyramidality angle (π) for the XML_4 square pyramid with the smallest S(TBP) value for a given bond length ratio M–X/M–L. (b) Minimum S(TBP) value of a square pyramid as a function of the bond length ratio.

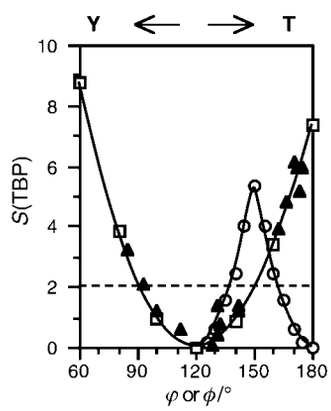

Fig. 5 TBP symmetry measure of a penta-coordinate complex as a function of the bending distortion θ involving only equatorial ligands (squares) keeping $\sigma = 90°$ (**b**, left). The symmetry measures corresponding to the Berry pathway, in which σ and ϕ are simultaneously varied (**a**), are also represented (circles) for comparison. Solid triangles correspond to homoleptic $[ML_5]$ complexes or MX_5 fragments in extended solids with one bond angle larger than 170° (data deposited as Supporting Information, Table S14).

Non-Berry angular distortions

In addition to the Berry pathway that takes a TBP to a SP, other angular distortions are relevant for the discussion of families of complexes with bi- or poly-dentate ligands. We will describe first the different distortions and their effect on the symmetry measure from a geometrical point of view, and discuss later the structures of several families of complexes.

Equatorial Y or T distortions

The first distortion we consider is the displacement of two equatorial groups keeping the two axial and one equatorial ligands fixed, calibrated by changes in the angle θ from its value in the ideal TBP (120°). It corresponds to an R_6 (E') distortion coordinate giving place to Y or T configurations of the equatorial ligands (**b** in Chart 2). The effect of such distortion on the symmetry measure is presented in Fig. 5 (squares, left branch). The Y distortion corresponds to the distortion coordinate $-R_6$ (E'), through which the unique bond angle θ decreases from that of the ideal TBP (120°) while the two equivalent angles γ become larger than 120°. Such distortion results in an increase of S(TBP), indicative of the loss of trigonal symmetry.

The opposite distortion increases θ and takes the equatorial ligands to a T configuration. The effect of such distortion on the CSM corresponds to the right branch of the curve presented in Fig. 5 (squares). A surprising result is that, for the same degree of distortion, the Y shape is farther from the TBP than the T one, as indicated by the asymmetric nature of that curve. It is interesting to compare the dependence of S(TBP) on θ for the T distortion with the evolution of the same parameter

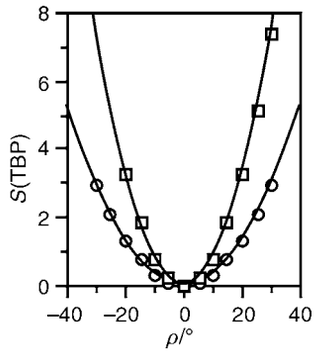

Fig. 6 Symmetry measure of ML_5 as a function of the off-axis displacement of one (circles) or two (squares) axial ligands, with the equatorial bond angles kept fixed at 120° (**c**,**c′**).

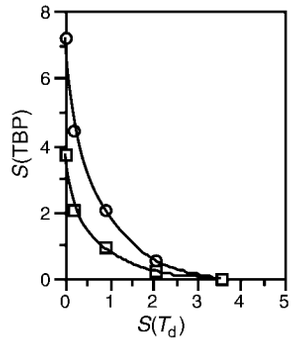

Fig. 7 Scatterplot of the TBP and tetrahedral symmetry measures for the XML_3 group of a XML_3Y molecule as it is distorted from the perfect TBP through an umbrella coordinate **d**, with all distances constant (squares), or simultaneously increasing the X–M bond distance up to an M–X/M–L ratio of 2.0 : 1 for $\omega = 110°$ (circles).

as a function of the angle ϕ (**a**) through the Berry pseudorotation (circles). Since in the Berry pathway the L_{ax}–M–L_{ax} bond angle decreases simultaneously to the increase of ϕ, one should not be surprised that TBP symmetry is lost earlier than with the T distortion. However, for $\phi = 150°$ the Berry distortion reaches a maximum CSM value of 5.37 and decreases again until the pseudorotated TBP is generated at $\phi = 180°$. In contrast, the T distortion continues to loose symmetry until an SP with $\pi = 90°$ ($\theta = 180°$) is reached, for which S(TBP) = 7.34. Notice that the structures **b** with $\theta > 120°$ have values of the angular parameter τ smaller than 1, even if these structures are farther away from the SP than the TBP itself. In summary, neither the symmetry measure, nor the angular parameter distinguish the Berry distortion from the T or Y distortions of the equatorial ligands. As an example, the dashed line in Fig. 5 indicates four structures with S(TBP) = 2.0. Structures having the same $S(G)$ value can be identified because symmetry is treated on a quantitative level and are termed *isosymmetric*.[3] Two such structures are along the Berry pathway, one presents a T distortion, and the fourth one a Y distortion of the equatorial ligands.

An illustration of the existence of crystal structures along such a distortion path is given in Fig. 5, where we have plotted the symmetry measures (provided as Supporting Information, Table S14) for those molecules of our reference set with $\sigma \geqslant 170°$ that show an approximate C_{2v} symmetry with a unique equatorial angle θ (solid triangles). The experimental data nicely follows the ideal behavior for Y- and T-equatorial distortions. The point at $\theta = 130°$ corresponds to $Cu_2O(SO_4)$[82] and presents a higher symmetry measure (1.39) than corresponds to its unique angle θ because of the differences in Cu–O bond distances (2.24 and 1.92 Å).

Reverse Berry distortion

A relevant distortion is that obtained by bending the two axial ligands in the direction opposite to the square pyramid (**c**) by an angle ρ each, in what has been termed *the reverse Berry pathway*. It corresponds to the R_7 (E') coordinate and would ultimately lead to an edge-capped tetrahedron (ECT). Although this structure has been referred to in the literature as edge-bridged tetrahedron,[83] it is common practice to use the term *capping* to indicate the position of a ligand relative to a polyhedron and qualify as bridges those ligands linking two different metal atoms. In such a distortion, the three equatorial ligands are kept fixed and only the axial ones are displaced. To simplify the discussion we analyze first the case in which the off-axis distortion affects only one axial ligand. The effect of such distortion on the symmetry measure is presented in Fig. 6. Notice that we take positive values of ρ for the Berry distortion and negative values for the reverse Berry distortion. The symmetric nature of the parabola in Fig. 6 around $\rho = 0°$ is not surprising, since any displacement of a ligand from a vertex of the ideal TBP that can be described by a vector $|\vec{Q}_k - \vec{P}_k|$ of the same modulus must present the same value of S(TBP), according to its definition (eqn. (1)). In the present case, the angular distortions defined by the angles ρ and $-\rho$ are just two particular cases of an infinite set of isosymmetric structures in which the off-axis axial bond is in any direction defined by a cone forming an angle ρ with respect to the trigonal axis of the TBP. The behavior of the TBP when the two axial ligands are shifted simultaneously by an angle ρ is qualitatively similar, only the S(TBP) values are larger for a particular distortion angle. As a consequence of the symmetric nature of the curve in Fig. 6, the symmetry measure is not able to differentiate between distortions of the L_{ax}–M–L_{ax} bond angles leading to a SP ($\rho > 0°$) or to an ECT ($\rho < 0°$). Notice also that, by definition, the S(TBP) value at $\rho = 30°$ (7.34) corresponds to a square pyramid with $\pi = 120°$ (Fig. 3).

Umbrella distortion

The umbrella displacement of the three equatorial ligands from the basal plane of the TBP is non-Berry distortion that corresponds to the R_4 (A''_2) mode. This mode can be described in a simple way by the simultaneous variation of the three bond angles ω (**d**). The case with $\omega = 90°$ corresponds to a perfect TBP with S(TBP) = 0, and larger values result as the equatorial ligands are displaced to either side of the equatorial plane. On the other hand, since the L_{eq}–M–L_{eq} angles decrease upon distortion, the angular parameter τ becomes larger than 1.0, providing a good hint for the existence of a non-Berry distortion. If one disregards the ligand X, the remaining ML_4 fragment approaches a tetrahedron as the ML_4X molecule is distorted from the TBP, even if the M–X and M–L distances are kept constant (Fig. 7, squares). The reader may suspect at this point that significant distortions along this path are unlikely to occur with all bond distances equal. An extreme example is provided by the $[ZnCl_5]^{3-}$ anion, that presents a very long Zn–Cl distance (3.77 Å) compared to four short ones (2.22–2.36 Å) and has been described more adequately as a tetrahedral anion with a van der Waals contact to a chloride ion.[80] The tetrahedral and trigonal bipyramidal symmetry measures, $S(T_d) = 0.26$ and S(TBP) = 4.8 are in excellent agreement with the chemical description. Hence, a more realistic pathway for the C_{3v} mode would combine the angular distortion **d** together with an elongation of the M–X bond. The interconversion between the tetrahedron and the TBP is represented by the changes in the two symmetry measures, as represented in Fig. 7 (circles).

The S_N2 pathway in Sn compounds

In two classical papers, Bürgi,[84] Britton and Dunitz[85] analyzed

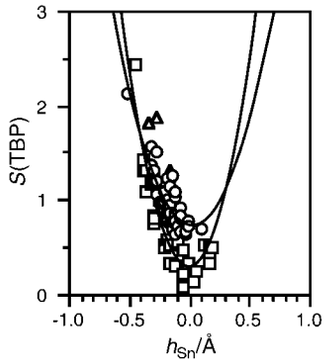

Fig. 8 Experimental TBP symmetry measure of the $XSnOC_3$ groups as a function of the displacement of the Sn atom out of the C_3 plane (h_{Sn}) for X = Cl (circles), Br (triangles) or N-donor ligand (squares).

the structures of Cd and Sn compounds of the type $XMYR_3$ that reflect the S_N2 pathway for ligand substitution with a Walden inversion (Chart 3). These authors showed that a good

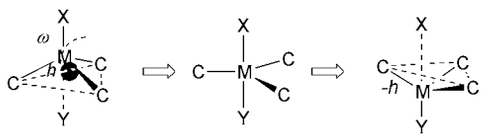

Chart 3

correlation exists between several bonding parameters: (i) the X–M–C average bond angle ω, (ii) the displacement of the M atom out of the C_3 plane (h_{Sn}), (iii) the difference between the X–M bond length and the atomic radii sum (Δx) and (iv) the difference between the Y–M distance and the corresponding radii sum (Δy). Such nice structural correlations seem adequate to investigate the feasibility of representing the combined changes in all these structural parameters by the TBP symmetry measure. Other families of Si compounds were also studied, but we choose as an example for the present study the large family of tin compounds with the $XSnOC_3$ core (where X is any Group 14–17 element).

The structural correlations first described by Bürgi [84] can also be seen in the much larger set of experimental structures of $XSnOR_3$ groups nowadays available (340 fragments of 187 compounds, see Supporting Information, Table S3), clearly tracing the S_N2 pathway for the substitution of the O-bonded group by the X-bonded group (or *vice versa*). Since the different structural parameters are correlated, we choose one of them, h_{Sn}, to describe the changes in the symmetry measure along the S_N2 coordinate. The results (Fig. 8) nicely show how the molecular structures approach the perfect TBP as the Sn atom moves into the plane formed by the three carbon atoms, and how the symmetry is lost again as the Sn atom moves to the other side of that plane. In contrast, a similar plot for the angular parameter τ (not shown) indicates that there is no correlation between h_{Sn} and τ. One can also see in this figure that Sn···O or Sn···X distances described in the Cambridge Structural Database as contacts may be much shorter than some others classified as bonds. The symmetry measure may therefore be a useful tool to decide whether a particular molecule should be considered as tetra- or penta-coordinate.

Since the two extremes of the S_N2 pathway are the unsubstituted $OSnR_3$ and $XSnR_3$ molecules, an alternative way of representing the associated structural changes consists in plotting the tetrahedricity of these groups (disregarding the O or X atom at a larger distance to Sn) as a function of the TBP symmetry measure. We choose to represent S(TBP) with a negative sign for those structures with the Sn atom displaced toward the X-bonded group (left hand side in Chart 3), and with a positive sign when it is displaced toward the Y-bonded group (right

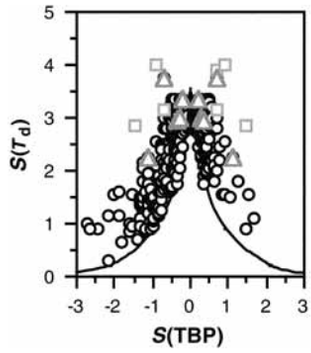

Fig. 9 Relationship between the tetrahedricity of the $SnOC_3$ or $XSnC_3$ fragment and the TBP symmetry measure of the $XSnOC_3$ core. For the measure of the tetrahedricity, the O or X atoms were chosen with the condition that the average O–Sn–C (or X–Sn–C) angle was larger than 90.00°. The squares correspond to those structures with one C–Sn–C bond angle larger than 135°, and triangles to structures with Sn–O or Sn–X bonds deviating more than 9° from the perpendicular to the C_3 plane. The data presented in this plot is deposited as Supporting Information (Table S3).

hand side in Chart 3). The behavior expected for an ideal umbrella distortion that keeps all bond distances constant (Fig. 9, continuous line) has been discussed above (Fig. 7). The corresponding plot for the experimental data (Fig. 9, circles) clearly reproduce the tendency toward a perfect tetrahedron at long Sn–O or Sn–X distances, indicated by $S(T_d) \approx 0$, as well as the gradual loss of tetrahedricity as the $XSnOC_3$ skeletons approach the trigonal bipyramid, S(TBP) = 0. It is noteworthy that the model distortion pathway represents a lower limit for the experimental tetrahedricity except for the geometries close to the perfect TBP.

The outliers in that plot clearly suggest the presence of an additional type of distortion. A look at the structural data indicates that in four such structures [86–89] (Fig. 9, squares) there is an unusually large C–Sn–C bond angle (larger than 135°) compared to those in all other structures (less than 130°). On the other hand, only a few structures [90–94] present a deviation of the Sn–O and Sn–X bonds from the trigonal axis larger than 9° (Fig. 9, triangles), thus accounting for the significant deviation of some points from the general behavior.

Bidentate ligands: $[Cu(bipy)_2X]^+$, $[Cu(phen)_2X]^+$ and $[M(dppe)_2X]^{n+}$ complexes

In this section we explore the effect of chelating ligands on the symmetry of penta-coordinate transition metal complexes. Extensive crystallographic work by Hathaway and co-workers has shown that Cu(II) complexes with bipyridine or phenanthroline with the general formula $[Cu(AA)_2X]$ (where AA is bipy of phen) give a variety of stereochemistries depending on the ligand X and on the counter ion.[95] In this section we analyze such stereochemical variation in the light of two of the non-Berry distortions of the TBP explored above for a model molecule. To that end, we analyze the structural data for those two families of compounds as well as for $[M(dppe)_2X]$ complexes, where M is any transition metal, dppe is 1,2-bis(diphenylphosphino)ethane or a topologically equivalent diphosphine, and X is a monodentate ligand.

One of the main characteristics of bidentate ligands in penta-coordinate complexes is that they may span an axial and an equatorial coordination position thus decreasing the corresponding A_{ax}–M–A_{eq} bond angles (η in Chart 4, **e**). In addition, even if such complexes may present a variety of geometries, from TBP to SP, the intermediate geometries cannot correspond to a Berry pathway, because of the constraints imposed by the chelate rings. The analysis of the experimental data indicates that the real structures can be derived from the chelated TBP *via* T- or Y-type distortions in the equatorial plane (**b**).

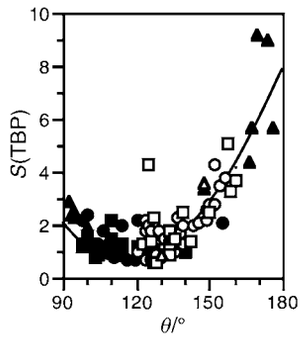

Fig. 10 TBP symmetry measure as a function of the bond angle θ in the Y and T distortion modes (**c**) for a model compound with a bite angle $\eta = 80°$ (solid line). Experimental data for $[Cu(bipy)_2X]^+$ (circles), $[Cu(phen)_2X]^+$ (squares) and $[M(dppe)_2X]$ (triangles) complexes are also shown. Filled symbols correspond to molecules along the asymmetric path **e**, empty symbols to the symmetric path **f**. The pertinent data is deposited as Supporting Information (Tables S4 and S5).

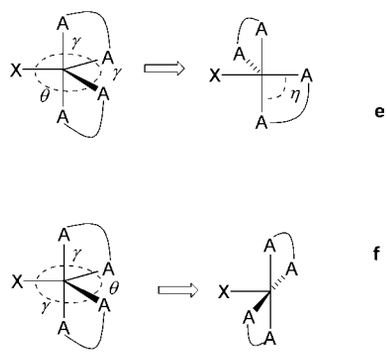

Chart 4

Because of the inequivalence of the A and X equatorial donors, the distortion in which the X–M–A_{eq} bond angle is the unique angle θ (**e**) is different to the analogous mode in which θ corresponds to the A_{eq}–M–A_{eq} angle (**f**). In the first case, the limiting SP at $\theta = 180°$ has the monodentate ligand X in a basal position, while in the second case X ends up in the axial position of the SP. No symmetry element is preserved in the first path (**e**) but a C_2 axis is retained in the second path (**f**) and we will refer to them as the asymmetric and symmetric distortions, respectively.

The evolution of *S*(TBP) for an ideal penta-coordinate molecule along the R_6 coordinate is shown in Fig. 10 (solid line). The bite angle (η in **e**) has been kept fixed at 80° to take into account that all the experimental structures of the $[Cu(bipy)_2X]^+$ and $[Cu(phen)_2X]^+$ complexes present bite angles close to that value. Similarly, the complexes of the type $[M(dppe)_2X]$ have values of η around 83° and in all cases smaller than 87°. The resulting curve is analogous to that discussed above (Fig. 5), shifted to higher *S*(TBP) values due to the distortion ($\eta < 90°$) introduced by the bidentate ligands.

The experimental data for compounds belonging to these three families are also represented in Fig. 10. One can appreciate that there is a general trend that is very well described by the equatorial T distortion for molecules along both the symmetric (filled symbols) and asymmetric (empty symbols) paths. As would be expected, the bipy and phen complexes show a similar behavior, with a large number of structures around the most symmetric one ($\theta = 120°$), but also many examples of strongly distorted TBPs. In these two families, the molecules along the asymmetric pathway **e** are T distorted, whereas those found along the symmetric path **f** are Y distorted. In other words, the monodentate ligand always occupies a vertex that gives the largest A–M–X bond angle. The structures of the dppe derivatives behave quite differently, with most of the structures analyzed showing strong distortions from the ideal TBP and two of them even having an almost perfect SP shape. With the available structural data it seems that the symmetric distortion pathway is more common than the asymmetric one for the dppe derivatives, and the symmetric distortion gives place to both Y- and T-type molecules, in contrast with the trends found for the bipy and phen complexes.

The representation of *S*(TBP) for this family of complexes as a function of the angular parameter τ shows a much poorer correlation than the plot in Fig. 10, indicating that the Berry pathway is not quite adequate to describe these structures, although one must be cautious not to generalize this conclusion to all complexes of the type $[M(chel)_2X]$ at the present time. The dispersion around the main trends in Fig. 10 is mostly associated with the presence of either a very long[96–106] or very short[107,108] M–X bond distance compared to the M–N ones. There is a clear exception to the general trend, at $\theta = 125°$ and *S*(TBP) = 4.28, corresponding to a salt of the $[Cu(phen)_2(H_2O)]^{2+}$ cation.[109] A look at that structure reveals that the aqua ligand is at quite a long distance from copper (2.73 Å) compared to other Cu–O distances in this family of complexes (shorter than 2.20 Å). Should this be considered as a non bonding distance? We can use the symmetry measures for the CuN_4 core to answer this question. The resulting tetrahedricity and square planarity measures are $S(T_d) = 16.19$ and $S(D_{4h}) = 4.91$, respectively. Even if these values are larger than *S*(TBP), they are close to those expected for a tetrahedrally distorted square planar molecule, as found in many tetra-coordinate Cu(II) complexes.[110] Probably one should describe it as a tetrahedrally distorted square planar $[Cu(phen)_2]^{2+}$ molecule, somewhat perturbed toward a trigonal bipyramid due to an incipient bond to the aqua ligand.

It is highly interesting to note that at least in two cases[102,111] one can find in the same crystal structure two chemically equivalent molecules, one of which is distorted along the asymmetric, another along the symmetric pathway. An additional interesting observation is that in no case a monodentate ligand occupies an axial position in an approximately trigonal bipyramidal structure, most probably because that stereochemistry would require a bidentate ligand to span two equatorial positions with a large bite angle close to 120°, whereas the largest bite angle experimentally found in the presently studied families of compounds is 84° for bipy, 86° for phen and 88° for dppe.

A very interesting example can be found in the structure[102] of the binuclear complex $[\{(bipy)_2Cu\}_2(\mu\text{-}ONO_2)](PF_6)_3$. The coordination sphere of one of the copper atoms (Cu1) is characterized by the following parameters: $\theta = 152.2$, $\gamma = 87.7°$ and *S*(TBP) = 4.32. These data are consistent with a geometry close to SP, generated from the TBP through the asymmetric pathway (Fig. 10). The angle γ practically corresponds to a vacant octahedron, whereas θ has not increased all the way to 180°, probably due to the different steric interactions of the axial N(bipy) atom with the equatorial N(bipy) and O(NO_3^-) atoms. The angular parameter, $\tau = 0.36$, adequately describes such a structure as a distorted square pyramid, but one should not interpret this value as indicating an intermediate geometry between TBP and SP, since the TBP symmetry measure expected for that angular parameter along a Berry coordinate (Fig. 2b) is much smaller than the experimental value.

The second copper atom in that molecule (Cu2) also has a N_4O coordination sphere, but with a quite different geometry. Its structural parameters (*e.g.*, $\theta = 108.8°$) clearly indicate that this structure is best described by the symmetric coordinate (**f**) leading to a square pyramid with the O atom in the axial position. However, the two angles that are expected to be approximately the same for such a distortion mode (γ), are significantly different in this case ($\gamma_1 - \gamma_2 = 12.5°$). Furthermore, two O–Cu–N bond angles are too small (79°) for either a square pyramid or a trigonal bipyramid. Its TBP symmetry measure, *S*(TBP) = 2.10, is too low for its angular parameter ($\tau = 0.04$), and

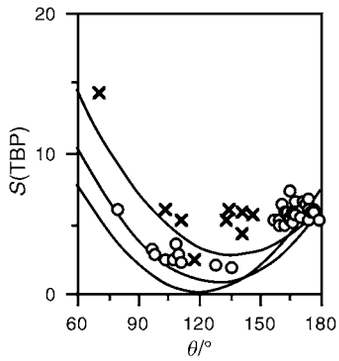

Fig. 11 TBP symmetry measure as a function of the large equatorial angle θ (Chart 5) for equidistance ML_5 polyhedra with $\eta = 70$, 80 and 90° (solid lines, from top to bottom). Experimental data for $[M(terpy)X_2]$ complexes with $65° < \eta < 75°$ (crosses) and $75° < \eta < 85°$ (circles) are also presented for comparison. Data deposited as Supporting Information (Tables S6 and S7).

suggests a large degree of TBP-ness that is inconsistent with the angular parameters. A closer examination of the corresponding structure tells us that the Cu1–O bond length is quite long (2.50 Å) compared to the Cu2–O bond in the same molecule (2.12 Å). If we consider the Cu2 atom to be tetra-coordinate, disregarding the oxygen atom at a long distance, what we find is that it has a geometry intermediate between square planar and tetrahedral, $S(D_{4h}) = 16.38$ and $S(T_d) = 5.04$, that corresponds nicely to the twist coordinate that interconverts the square planar and tetrahedral structures.[110] The small S(TBP) value of this structure should thus be considered as a geometric artifact that can be easily recognized from its unrealistic position in the scatterplot of S(TBP) and τ.

Tridentate ligands: terpyridine complexes

In terpyridine complexes, with general formula $[M(terpy)X_2]$, the two end nitrogen atoms of terpy occupy the axial positions of the ideal TBP, whereas the central nitrogen and the two X ligands occupy the equatorial position. The tridentate nature of terpy forces small N–M–N bond angles ($65.7 \leqslant \eta \leqslant 80.7$, see Chart 5). Since the three N atoms form part of the rigid tri-

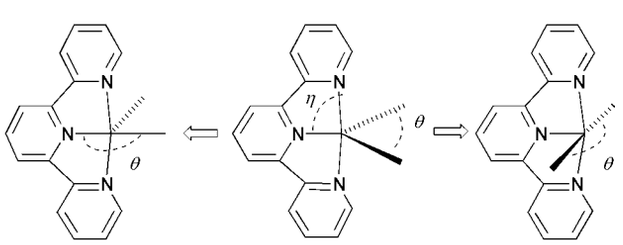

Chart 5

dentate ligand, the Berry pathway is not allowed and the angular parameter τ does not apply to this family of compounds. This can be seen in Fig. 11, where we represent the TBP symmetry measure as a function of θ at different bite angles η (solid lines). Besides the distortion from the ideal TBP induced by the tridentate ligand, in most cases the equatorial bond angles deviate from the perceptive 120°. Such distortions correspond to the Y- and T-modes discussed above, with the latter ultimately leading to a square pyramid. In some compounds, the distortion is such that X–M–X is the large equatorial angle, corresponding to a target SP in which one X atom occupies the apical position (**g**), akin to the distortion **e** discussed above for bis(bidentate) complexes. Other compounds appear along the pathway of conversion of the TBP into an SP with the central N atom in the apical position (**i**). To simplify the discussion, we consider from here on only the first coordination sphere and do not differentiate the two distortion pathways. The scatterplot of S(TBP) and θ (Fig. 11) for the experimental data reveals only a few structures with nearly TBP geometry ($\theta \approx 120°$), a handful of structures approaching the two SP's ($\theta \approx 180°$), and some Y distorted ($\theta < 120°$) ones. An extreme distortion corresponds to a silver compound[112] in which the X positions are occupied by the bidentate bipy ligand, and θ is therefore the bite angle (71°). Its very large S(TBP) value though, is consistent with the equatorial distortion pathway for $\eta \approx 70°$ ($\eta_{exp} = 68.7°$).

Complexes with tripod ligands

Since tripod ligands are topologically well adapted for TBP coordination, we analyze here the structures of pentacoordinate complexes of the type [M(tripod)X], where tripod is a tetradentate N-donor ligand with ethyl arms, *e.g.*, $N(C_2H_5NR_2)_3$, X is any monodentate ligand, and M is any transition metal (**j**, Chart 6). In most of these compounds, the metal atom

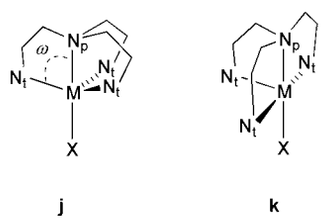

Chart 6

is out of the equatorial plane of the TBP, away from the pivotal atom of the tripod (N_p in **j**). Hence, the X–M–N_t angles (ω) are always found to be less than 90° ($72 < \omega < 87°$), with the consequent loss of the D_{3h} symmetry. As expected from the general effect of pyramidality around an atom on the axial bond distances,[113,114] a clear correlation appears between ω and the axial M–N bond distance (the bond distance ratio $M–N_p/M–N_t$ varies between 0.92 and 1.26), even if there is some dispersion around the main trend (Fig. 12a), undoubtedly associated to the varied nature of the M and X atoms and of the tripod substituents in the set of structures considered (data provided as Supporting Information, Table S8).

The correlation between ω and S(TBP) suggests a tendency to dissociation of the pivotal N atom at small values of ω, that would result in a tetrahedral $MX(N_t)_3$ core, but are prevented by the chelate effect associated with the legs of the tripod. Hence, it is worth studying whether the loss of TBP-ness induced by decreasing ω is associated with an increase in the tetrahedricity of the $MX(N_t)_3$ group. The corresponding scatterplot for the experimental structural data is presented in Fig. 12b, together with the calculated curve for a model molecule ML_5 with all bond distances equal. The first eye-catching result is that two trends seem to coexist. On the one hand, most of the points (shown as circles) follow the expected trend, consistent with a distortion mode that approximately preserves the C_{3v} symmetry: the tetrahedricity increases from right to left at the expense of the loss of trigonal bipyramidality. On the other hand, there are a few points (shown as black triangles) that present a practically linear correlation, and indicate that both tetrahedricity and TBP-ness are simultaneously lost from left to right (the continuous line is a least squares fitting). Once the two families of compounds are identified, an analysis of the structural parameters indicates that the triangles correspond to structures distorted toward a square pyramid in which one of the N_t atoms is in the apical position (**k**). All these structures have practically planar $M(N_t)_3$ groups (the sum of bond angles is larger than 356° in all cases) and there is one $N_t–M–N_t$ bond angle larger than 129°. In contrast, in the rest of the structures the largest $N_t–M–N_t$ bond angle is smaller than 127°. Interest-

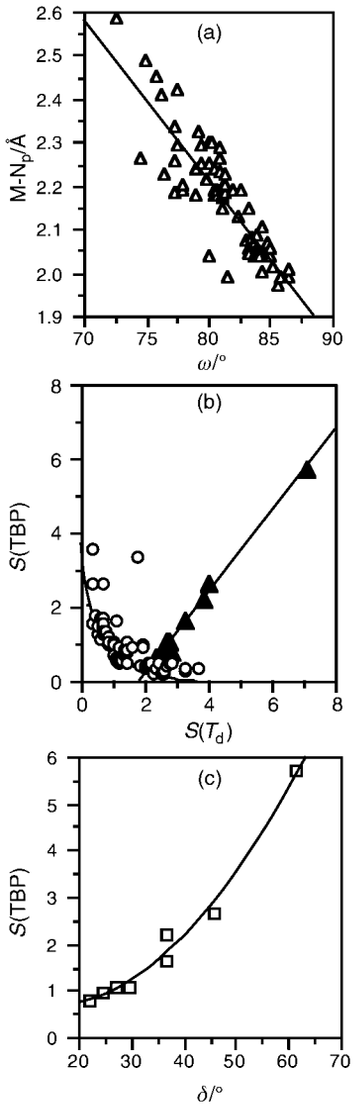

Fig. 12 (a) Axial M–N_p bond distances as a function of the average X–M–N_t bond angle (ω in **j**) in complexes of the type [M(tripod)X]. (b) Scatterplot of the trigonal bipyramidal and tetrahedral symmetry measures for the same compounds, where the triangles represent those structures with a practically planar $M(N_t)_3$ group (*i.e.*, $\Sigma(N_t–M–N_t) > 356°$) and one $N_t–M–N_t$ angle larger than 129°. The straight line corresponds to a least squares fitting. (c) TBP symmetry measure as a function of the difference between the largest and smallest $N_t–M–N_t$ bond angles for complexes of the type [M(tripod)X] with a practically planar $MN_p(N_t)_2X$ core.

ingly, all the structures showing a distortion toward the square pyramid correspond to copper complexes. For such compounds that follow path **k**, the TBP symmetry measure is nicely correlated with the difference δ between the largest and smallest $N_t–M–N_t$ bond angles (Fig. 12c).

One structure[115] seems to be anomalous in the sense that it follows neither of the general trends, with $S(T_d) = 1.71$ and $S(\text{TBP}) = 3.39$. A look at the structural data shows that in this cationic complex, $[Hg(N\{C_2H_5NMe_2\}_3)Ph]^+$, the three arms of the tripod ligand are held at quite long distances from the Hg atom (2.7 Å), compared to M–N_t distances shorter than 2.30 Å (typically 2.05 Å) in all other structures. Since the Hg–N_p and Hg–C distances are 2.27 and 2.09 Å, respectively, it seems reasonable to consider the Hg atom as bi-coordinate with three *contacts* to the arms of the tripod. Such a description is in agreement with electron counting rules that prescribe 14 valence electrons for the metal atom in a linear complex, whereas a penta-coordinate Hg(II) ion would have 20 valence electron counts, two electrons in excess of the 18-electron rule.

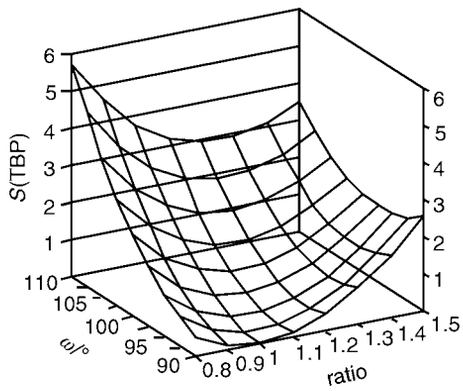

Fig. 13 S(TBP) as a function of the average bond angle ω and the $M–N_p/M–N_t$ distance ratio for the MN_4X group in **d**.

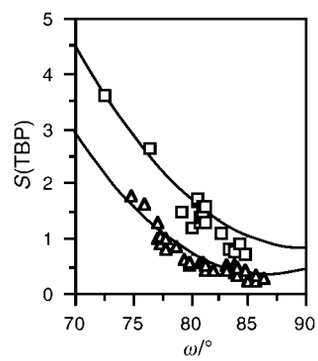

Fig. 14 Ideal behavior of S(TBP) as a function of the umbrella distortion defined by the bond angle ω in [M(tripod)X] complexes with approximately C_{3v} symmetry (**d**) at $M–N_p/M–N_t$ distance ratio of 1.2 : 1 (upper line) and 1.0 : 1 (lower line). Experimental data for X = Cl, Br are represented by squares, those for X = N-donor ligand by triangles.

The M–X distances also show some dispersion within this family, with $M–X/M–N_t$ distance ratios between 0.77 and 1.22 : 1. Hence, the loss of trigonal bipyramidal symmetry in the complexes with tripod ligands is associated with changes in three structural parameters: the bond angle ω and the $M–N_p/M–N_t$ and $M–X/M–N_t$ distance ratios. Ideally, such dependence is illustrated in Fig. 13, where S(TBP) is represented as a function of ω and the $M–N_p/M–N_t$ bond distance ratio, with the M–X and M–N_t bond distances kept constant at 2.25 Å. There one can see that as ω increases the minimum S(TBP) value increases and is shifted to larger distance ratios. Two cross-sections of the analogous surface obtained with $M–N_p/M–N_t = 1.2$ are shown in Fig. 14 (solid lines), together with the experimental data for those compounds that retain an approximate C_{3v} symmetry in which the monodentate ligand is a halide (open squares) or a N-donor ligand (open triangles). An interesting result is that the least-squares parabola (not shown) for the experimental points corresponding to compounds in which X is a halide extrapolates to a perfect trigonal bipyramid ($S = 0.0$) at $\omega = 90°$.

The reverse Berry distortion and the edge-capped tetrahedron

In a previous section we have seen that the symmetry loss from a perfect ML_4X TBP induced by the reverse Berry distortion **c**[83] would ultimately give place to an edge-capped tetrahedron (ECT), in which the pivotal ligand (X in **c** and **c′**) occupies the capping position (Fig. 6). The inverse of this coordinate represents a possible pathway for the association of a fifth ligand to an edge of a tetrahedral molecule. Here we analyze the changes in the TBP-ness and tetrahedricity of both the ML_4X and ML_4 polyhedra. A scatterplot of the two symmetry measures for the

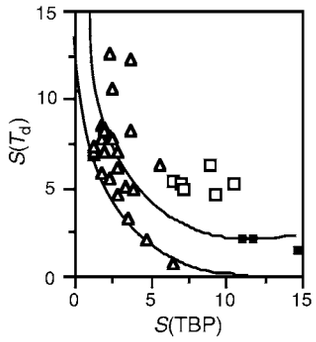

Fig. 15 Scatterplot of the TBP and T_d symmetry measures for the XML_4 and ML_4 fragments of penta-coordinate complexes with geometries along the reverse Berry distortion **c**, where ρ varies between 0 and 35° (lower line). Distortions that keep the equatorial angles constant at 120°, or in which the equatorial L–M–L angle decreases from 120 to 109° as ρ increases, give the same curve. The upper line corresponds to a model in which the equatorial angles are kept constant at 140°. Experimental data presented also for ML_5 complexes with monodentate ligands (triangles), $[MH_2XCp_2]$ complexes (white squares) and $[MX_2HCp_2]$ complexes (black squares). References and numerical data are provided as Supporting Information.

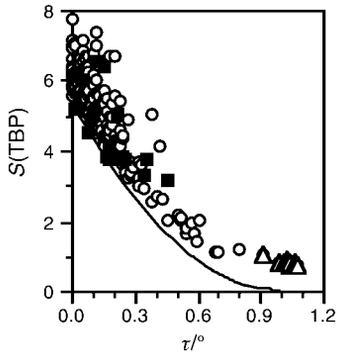

Fig. 16 TBP symmetry measure as a function of the angular parameter τ for vanadium compounds. The solid line corresponds to the Berry coordinate. Experimental data displayed correspond to $[OVL_4]$ (circles) or [OV(tripod)] (triangles) complexes, and to vanadium oxides (squares) and are provided as Supporting Information (Tables S11 and S12).

conversion of a TBP into an ECT is presented in Fig. 15 for three ideal paths. In all three paths the angles ρ were varied from 0° (ideal TBP) to 35°, whereas the capping atom X has been disregarded to obtain the tetrahedricity measure. In the first path all other structural parameters were kept fixed as in the ideal TBP. In a second pathway, the equatorial bond angles were varied simultaneously with ρ. Although the two symmetry measures at a particular angle ρ give different values for these two distortion coordinates, the resulting S(TBP) *vs.* $S(T_d)$ curves are indistinguishable (Fig. 15, lower line). In the third path, the equatorial L–M–L angle was kept fixed at 140° for reasons to be explained below (Fig. 15, upper line).

Comparison of the experimental data for some d^0 compounds with monodentate ligands proposed as examples of ECT structures[77,83] indicate that our model pathways represent reasonably well the distortion coordinate, although the experimental tetrahedricites are smaller, *i.e.*, the $S(T_d)$ values larger, than in the ideal paths. The VO_5 groups in some vanadium(v) oxides are also found along this line and the pertinent data[116–118] are also presented in Fig. 15. Even if the present approach does not require the metal–pivotal ligand bond to be cleaved to achieve the perfect tetrahedron, Fig. 15 (triangles) clearly shows that most of the test structures are much closer to the ideal TBP than to a tetrahedron. An interesting case is that of the organometallic complex dibenzyl(methylamine-*N*,*N*-bis(methylene-*o*-naphthylene))zirconium(IV),[119] in which the tridentate nature of the aminobis(naphthylene) ligand seems to favor a structure that is practically isosymmetric with respect to the tetrahedron and the trigonal bipyramid: S(TBP) = 3.44 and $S(T_d)$ = 3.26. The nicest example of an edge-capped tetrahedron that we have been able to identify is given by the $RuSi_5$ groups in $NdRuSi_2$ (S(TBP) = 6.47, $S(T_d)$ = 0.82).

Even if the η^5-Cp ligand is electronically tridentate, it can be considered geometrically as a single ligand. Hence, the structures of the family of d^0 $[ML_2XCp_2]$ complexes, related to the highly interesting metallocene catalysts for the stereospecific polymerization of α-olefins, can be analyzed in terms of their TBP symmetry measures. Ward *et al.*[83] used such an approach to map the reverse Berry pathway in that family, which might be at the root of the catalytic stereospecificity. In this family of compounds, the centroids of the Cp rings (labeled c from here on) can be identified as the equatorial ligands in **c**. The c–M–c angles are significantly larger than in the ideal TBP (around 140°), and the correlation between TBP-ness and tetrahedricity expected with such angle fixed upon varying ρ is represented in Fig. 15 (upper solid line). Because of the large equatorial angle, neither the ideal ML_2Xc_2 TBP nor the ideal ML_2c_2 tetrahedron can be reached. The experimental data clearly show the loss of trigonal bipyramidality (*i.e.*, higher S(TBP) values), with respect to analogous complexes having σ-bonded ligands. Nevertheless, there are two distinct groups of structures. On the one hand we have the complexes of the type $[MH_2XCp_2]$ (where X is a ligand with a P, Si, Ge or Sn donor atom), whose MH_2c_2 cores are still far from the tetrahedron (Fig. 15, white squares). On the other hand, there are a few $[MX_2HCp_2]$ compounds (X is a Si or P donor ligand), which appear to be as close to the tetrahedron as a molecule with a wide c–M–c angle can be (Fig. 15, black squares). The large values of $S(T_d)$ found for the MH_2c_2 cores have to do also with the important difference between the M–H and M–c distances.

Vanadyl complexes and vanadium oxides

Penta-coordination is very common for oxides of vanadium-(IV) and -(V),[120] although tetra-coordination can also be found for V(V) and hexa-coordination for V(IV). The molecular counterpart of such oxides is provided by the penta-coordinate vanadyl complexes $[OVL_4]$, most of which are square pyramidal.[121] Vanadium(V) sites in enzymatic systems, which are attracting an increasing interest,[122] present crystallographic evidence of the TBP geometry around penta-coordinate vanadium atoms. Furthermore, a variety of vanadyl complexes (vanadyl, VO^{2+}) are being intensely investigated due to their insulin-mimetic activity.[123,124] A continuous symmetry analysis of such compounds will show how the local symmetry around the vanadium atom offers a common playground for the description of the structures of both molecules and solids.

A plot of the trigonal bipyramidal CSM as a function of the angular parameter τ for complexes of the type $[OVL_4]$ and for some vanadium oxides (Fig. 16) reveals several trends. (i) The vanadyl complexes and the vanadium oxides show the same qualitative behavior, approximately described by the Berry pathway. (ii) The structures are most often close to the square pyramid, with a number of them showing varying degrees of distortion toward the trigonal bipyramid, but only a few molecules are close to the ideal TBP. (iii) For the nearly perfect SP structures ($\tau \approx 0.0$), the TBP symmetry measure presents values between 5.5 and 8.0 due to the varying degrees of pyramidality (experimental values $98 < \pi < 112°$). (iv) With a few exceptions, only those vanadyl complexes with a tripod ligand can be clearly described as trigonal bipyramidal. The structure closest to TBP without a tripod ligand is that of the binuclear compound $[\{(ClC_2H_4O)_2OV(\mu\text{-}OC_2H_4Cl)\}_2]$.[125] (v) The fact that the CSM for the tripod complexes is in all cases larger than 0.4 is due to the umbrella distortion **d** discussed

above. (vi) One of the most successful insulin-mimetic vanadyl complexes, bis(maltolato)vanadyl (BMOV) presents an intermediate geometry[126] characterized by $S(\mathrm{TBP}) = 4.82$. If molecular symmetry at the vanadium atom is of any relevance for the biological activity of BMOV, Fig. 16 tells us that it should be easy to find related complexes with different chemical composition and similar symmetry, given the abundance of structures around that value of S(TBP).

Coordination mode of the nitrosyl ligand in $\{MNO\}^8$ complexes

The biological relevance of nitric oxide and its reactivity toward metalloproteins makes the study of the nitrosyl metal complexes a very active research area. The NO ligand can be found bound to a transition metal atom giving either a linear or a bent M–N–O fragment.[127,128] In the linear conformation, the ligand is counted as NO^+, isoelectronic with CO, whereas a strongly bent ligand is counted as NO^-. Hence, the orientation of the nitrosyl ligand has a strong implication on the formal oxidation state of the metal. To avoid ambiguities when referring to the number of valence electrons of a particular complex, the $\{MNO\}^n$ formalism has been introduced,[129] where n is the sum of electrons in the metal d and in the NO π^* orbitals. As an example, $[Mn(CO)_4NO]$ would be referred to as a $\{MnNO\}^8$ complex. In this section we consider only the $\{MNO\}^8$ compounds, that may be counted either as NO^+ complexes of d^8 or as NO^- derivatives of d^6 metals. Since the trigonal bipyramid is preferred for d^8 and the square pyramid for d^6 penta-coordinate complexes, it has been shown[79,130] that the bending of the M–N–O group is associated to the degree of distortion from the trigonal bipyramid to the square pyramid (Chart 7). It was also

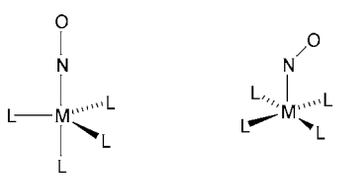

Chart 7

proposed that there is not an either/or situation between the two structures, but rather a continuum of structure, formal charge of NO and oxidation state of the metal atom. Since we now have precise ways to measure the deviation from the TBP geometry, we wish to analyze the structure of such compounds from the point of view of the symmetry measure. To that end we carried out a structural database search[131] of penta-coordinate nitrosyl complexes, limited to compounds with only one nitrosyl ligand per metal atom, with no disorder in the crystal structure, and with an $\{MNO\}^8$ electron configuration.

In Fig. 17 we present the S(TBP) *vs.* τ plot for this family of compounds, together with the ideal curve for the Berry pseudorotation. The S(TBP) values for the experimental structures, larger than for the Berry pathway, indicate the presence of non-Berry distortions. However, the essentials of the symmetry changes are reasonably described by the Berry distortion coordinate. The distribution of the experimental data suggests that there are two minima in the potential energy surface, one with the SP and one with the TBP geometry around the metal atom. The scarcity of points with intermediate symmetry, at $S(\mathrm{TBP}) \approx 3$, suggests the existence of a barrier for the interconversion between the two polyhedra. This is clearly seen if we plot the M–N–O angle as a function of the symmetry measure (Fig. 17b). As expected, the SP geometries present small M–N–O bond angles, whereas larger values are observed for the TBP molecules. Interestingly, there seems to be a forbidden region of M–N–O bond angles: for small distortions, $S(\mathrm{TBP}) \leqslant 4$, only small deviations from linearity can be appreciated (M–N–O > 158°). As the distortion towards the square pyramid goes beyond the $S(\mathrm{TBP}) = 4$ threshold, the NO flips to a strongly bent (M–N–O < 136°) position.

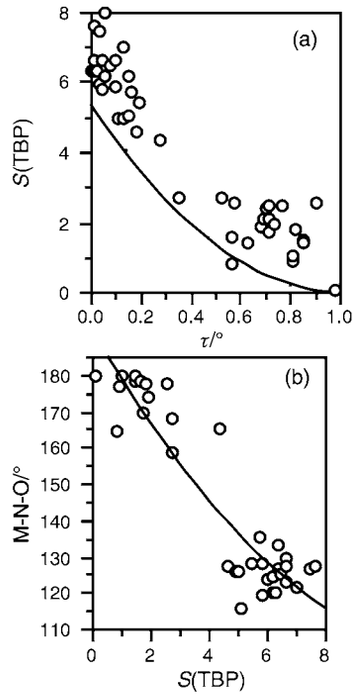

Fig. 17 (a) Scatterplot of the TBP symmetry measure and the angular parameter τ for the structures of $L_5M(NO)$ complexes with $\{MNO\}^8$ electron configuration (circles). The values corresponding to the Berry pathway are also shown for comparison (continuous line). (b) M–N–O bond angle as a function of the TBP symmetry measure of $L_5M(NO)$ complexes.

Main conclusions

Several aspects of the structural chemistry of penta-coordinate molecules have been analyzed in the light of the TBP continuous symmetry measures. Bond length distortions of the trigonal bipyramid in which the long/short bond distance ratio is at most 1.2 : 1 result in increases of the S(TBP) values of less than 0.9 units. The upper limit of the TBP symmetry measure for distortions involving the stretching of a given number of bonds are similar and increase with the number of stretched bonds. Also, for distortions in which the same number of bond lengths are stretched to the same extent, the S(TBP) value is larger for the distorted molecule that keeps more symmetry elements.

The Berry pseudorotation pathway is well described by both the angular parameter τ and the trigonal bipyramidal symmetry measure S(TBP). We have found it useful to represent the different distortion coordinates as scatterplots of the two parameters. The idealized Berry pathway used in this paper for penta-coordinate molecules with five identical bond distances is represented by S(TBP) values between 0.000 for the ideal trigonal bipyramid and 5.374 for the ideal square pyramid having bond angles of 105°. Experimental structural data for the homoleptic transition metal complexes and for EPh_5 molecules of Group 15 elements are distributed along the Berry coordinate characterized by $0.0 < S(\mathrm{TBP}) < 5.4$, except for those structures with a nearly perfect SP structure ($\tau \approx 0$) that show S(TBP) values between 5.4 and 7.8. The variation in the symmetry measures of the square pyramids is associated to their different pyramidality (*i.e.*, $\pi = L_{ax}$–M–L_{eq}) angles. The square pyramid closest to a trigonal bipyramid is that with $\pi = 104.9°$ and an axial/basal bond distance ratio of 1.05 : 1, for which $S(\mathrm{TBP}) = 5.347$. A conclusion is that the Berry coordinate adopted in this paper practically corresponds to a maximum TBP-ness pathway. While the CSM approach is able to

discriminate between different square pyramids, the angular parameter τ presents the same value for any C_{4v} square pyramid. The structural data for square pyramidal homoleptic complexes (with five similar bond distances) and those for molecules with shorter axial distances, $[MO_4]$ and $[MN_4]$ are neatly segregated in a plot of S(TBP) as a function of the pyramidality angle π.

Different angular distortions can give place to isosymmetric structures, *i.e.*, structures with the same value of S(TBP). As an example, angular distortions that result in T or Y arrangements of the equatorial ligands are isosymmetric with each other, with a structure along the Berry pathway and with another one along the reverse Berry coordinate. For the off-axis angular distortion of an axial ligand, an infinite set of isosymmetric structures can be defined that are described by the cone that the M–L axial bond forms with the trigonal axis of the equatorial ligands.

The study of the reverse Berry distortion in ML_5 complexes shows that it affects the TBP symmetry measure in much the same way as the Berry coordinate. This is a clear example of how symmetry measures provide a numerical indication of the distance of a particular structure to an ideal TBP, but not on the direction in which it is distorted. A similar behavior is expected for the angular parameter τ, that cannot discriminate between a Berry and a reverse Berry distortion. The tetrahedricity of ML_4 fragments of penta-coordinate molecules in several reference structures shows that these cannot be adequately described as edge-capped tetrahedra (ECT). The catalytically interesting metallocenes of d^0–d^2 metal ions and formula of the type $[MCp_2L_2X]$ can be regarded as penta-coordinate if one considers the centroid of each cyclopentadienide ring as a single ligand. The $S(T_d)$ values for the MCp_2L_2 groups in such complexes has been found to be quite small and the S(TBP) values large, indicating that they can be reasonably described as edge-capped tetrahedra.

An angular parameter τ larger than 1.0 provides a good hint for the existence of an umbrella distortion, typical of complexes with tripod ligands. Such a distortion coordinate also allows one to follow the gradual conversion of a tetrahedron into a TBP through the addition of a fifth ligand at a face of the tetrahedron and *vice versa*. Such interconversion can be best analyzed by a scatterplot of the tetrahedricity of the four short bonds as a function of the TBP-ness of the putative penta-coordinate molecule. As an example of the umbrella distortion we have analyzed the changes in the symmetry measure along the S_N2 coordinate depicted by the structures of $XSnOR_3$ groups. The S(TBP) values are well correlated with the changes in bond lengths and angles around the Sn atom, whereas no correlation is found between the angular parameter τ and the structural data. The TBP symmetry measure can be therefore used as a single parameter representing the structural changes along the S_N2 pathway for the substitution of the O-bonded group by the X-bonded group or *vice versa*. Sn···O or Sn···X distances described in the literature as contacts are much shorter than some classified as bonds, and our results suggest that the comparison of the $S(T_d)$ and S(TBP) values can be of help in deciding whether to consider a particular molecule as tetra- or penta-coordinate. In this case, the experimental data shows no structural discontinuity between tetra- and penta-coordinate Sn species, clearly indicating the arbitrariness of the assignment of a particular coordination number in these compounds.

Complexes with tripod ligands [M(tripod)X] show two different types of distortion from TBP, easily identifiable through the symmetry measures. An umbrella distortion mode is characterized by an increase in S(TBP) of the MN_4X core with a concomitant decrease in the $S(T_d)$ value for the MN_3X fragment in which the pivotal N atom is disregarded. A number of Cu(II) complexes, however, present a T-type distortion from TBP to SP that results in a simultaneous increase of the two symmetry measures. The position of a particular structure with an umbrella distortion in the scatterplot of S(TBP) and $S(T_d)$ is affected significantly but to a lesser extent by the ratios between axial and equatorial bond distances.

From the study of the symmetry measures of families with bi- and tri-dentate ligands we can conclude that complexes such as $[Cu(bipy)_2X]$, $[Cu(phen)_2X]$ and $[M(terpy)X_2]$ are not adequate models to describe the Berry pseudorotation pathway as proposed in the literature.[132] The deformation from TBP to SP in these complexes occur through two alternative pathways. The bipy and phen derivatives are preferentially found along a C_s pathway that takes the coordination polyhedron to a square pyramid with the monodentate ligand in a basal position, whereas the dppe complexes occur mostly along a C_{2v} coordinate leading to a SP with the monodentate ligand in the axial position. Complexes of the type $[Cu(terpy)X_2]$ are found in either of the two distortion modes.

Other families of compounds studied comprise vanadyl and metal nitrosyl complexes. The vanadyl complexes and VO_5 fragments in the extended structures of V(IV) and V(V) oxides all behave in a similar way, with a clear preference for square pyramids with some degree of distortion toward the TBP along the Berry coordinate. The structures closest to a trigonal bipyramid are those with a tripod ligand. According to the electronic preference of penta-coordinate d^8 complexes for the TBP and of d^6 complexes for the SP geometry, the metal nitrosyl complexes with $\{MNO\}^8$ configuration show a nice correlation between S(TBP) and the M–N–O bond angle. Compounds closer to the TBP (*i.e.*, S(TBP) $\leqslant$ 4.4) present large M–N–O bond angles (>158°), and those closer to the SP (*i.e.*, S(TBP) $\geqslant$ 4.6) present small bond angles (<136°). An interesting result is that structures with intermediate bond angles seem to be forbidden.

A common feature of all the distortions and families of structures analyzed is that the scatterplots of symmetry measures relative to two different polyhedra or representation of a symmetry measure as a function of some structural parameter allow for an easy identification of anomalous structures. In some cases these anomalies have been shown to be due to an inadequate assignment of coordination number of the metal atom. The symmetry measures have also been shown to be interesting parameters to describe reaction coordinates.

Acknowledgements

The authors gratefully acknowledge many enlightening discussions with D. Avnir, as well as authorization to use the sym_he computer code. Help from S. Keinan and M. Pinsky for the installation and modifications to that program is also highly appreciated. This work has been supported by the Dirección General de Enseñanza Superior (DGES), project PB98-1166-C02-01. Additional support from Comissió Interdepartamental de Ciència i Tecnologia (CIRIT) through grant SGR99-0046 is also acknowledged. S. A. thanks the Dozor Foundation (Israel) for a Visiting Professorship that acted as a catalyst for the research reported in this paper.

Appendix

The symmetry measures were calculated with the computer program sym_he developed by the group of D. Avnir. The collections of structural data were obtained through systematic searches of the Cambridge Structural Database (version 5.18).[131] Searches were restricted to crystal structures with no disorder and $R < 10\%$. For the analysis of large number of structural data from the Cambridge Structural Database we used the program csm_ctrl developed by us. Tables of REFCODES, relevant structural information and calculated symmetry measures are deposited as Supporting Information.

A search was conducted for structures with a penta-coordinate Sn atom, with the X (any atom belonging to Groups 14–17) and O atoms in axial positions (*i.e.* the O–Sn–X angle was required to be larger than 169 degrees), or for a formally tetra-coordinate Sn atom with the $XSnC_3$ core and a contact to O at less than 3.0 Å, or with the SnC_3O core with a contact to X at less than 3.0 Å.

References

1 D. Avnir, O. Katzenelson, S. Keinan, M. Pinsky, Y. Pinto, Y. Salomon and H. Zabrodsky Hel-Or, in *Concepts in Chemistry: A Contemporary Challenge*, ed. D. H. Rouvray, Research Studies Press Ltd., Taunton, England, 1996.
2 H. Zabrodsky, S. Peleg and D. Avnir, *J. Am. Chem. Soc.*, 1992, **114**, 7843.
3 M. Pinsky and D. Avnir, *Inorg. Chem.*, 1998, **37**, 5575.
4 D. Avnir, S. Keinan, M. Pinsky and S. Alvarez, to be submitted.
5 A. W. Addison, T. N. Rao, J. Reedijk, J. van Rijn and G. C. Verschoor, *J. Chem. Soc.*, *Dalton Trans.*, 1984, 1349.
6 E. F. Epstein and I. Bernal, *J. Chem. Soc. A*, 1971, 3628.
7 L. P. Battaglia, A. B. Corradi, L. Antolini, T. Manfredini, L. Menabue, G. C. Pellacani and G. Ponticelli, *J. Chem. Soc.*, *Dalton Trans.*, 1986, 2529.
8 W. Clegg, D. A. Greenhalg and B. P. Straghan, *J. Chem. Soc.*, *Dalton Trans.*, 1975, 2591.
9 L. Antolini, G. Marcotrigiano, L. Menabue and G. C. Pellacani, *J. Am. Chem. Soc.*, 1980, **102**, 1303.
10 K. N. Raymond, D. W. Meek and J. A. Ibers, *Inorg. Chem.*, 1968, **7**, 1111.
11 I. Bernal, J. D. Korp, E. O. Schlemper and M. S. Hussain, *Polyhedron*, 1982, **1**, 365.
12 S. A. Goldfield and K. N. Raymond, *Inorg. Chem.*, 1971, **10**, 2604.
13 B. Scott and R. Willett, *Inorg. Chim. Acta*, 1988, **141**, 193.
14 B. Scott, U. Geiser, R. D. Willett, B. Patyal, C. P. Landee, R. E. Greeney, T. Manfredini, G. C. Pellacani, A. B. Corradi and L. P. Battaglia, *Inorg. Chem.*, 1988, **27**, 2454.
15 M. Duggan, N. Ray and B. J. Hathaway, *J. Chem. Soc.*, *Dalton Trans.*, 1980, 1342.
16 A. Wilk, W. Massa, C. Friebel and D. Reinen, *Z. Anorg. Allg. Chem.*, 1992, **608**, 88.
17 T. Glowiak and I. Wnek, *Acta Crystallogr.*, *Sect. C*, 1985, **41**, 324.
18 R. J. Majeste and L. M. Trefonas, *Inorg. Chem.*, 1974, **13**, 1062.
19 M. Herberhold, F. Wehrmann, D. Neugebauer and G. Huttner, *J. Organomet. Chem.*, 1978, **152**, 329.
20 A. Alvanipour, H. Zhang and J. L. Atwood, *J. Organomet. Chem.*, 1988, **358**, 295.
21 M. S. Corraine, C. K. Lai, Y. Zhen, M. R. Churchill, L. A. Buttrey, J. W. Ziller and J. D. Atwood, *Organometallics*, 1992, **11**, 35.
22 H. Ben Laarab, B. Chaudret, F. Dahan, J. Devillers, R. Poilblanc and S. Sabo-Etienne, *New J. Chem.*, 1990, **14**, 321.
23 B. A. Frenz and J. A. Ibers, *Inorg. Chem.*, 1972, **11**, 1109.
24 G. Kong, G. N. Harakas and B. R. Whittlesey, *J. Am. Chem. Soc.*, 1995, **117**, 3502.
25 B. Balbach, S. Baral, H. Biersack, W. A. Herrmann, J. A. Labinger, W. R. Scheidt, F. J. Timmers and M. L. Ziegler, *Organometallics*, 1988, **7**, 325.
26 R. Seidel, B. Schnautz and G. Henkel, *Angew. Chem.*, *Int. Ed. Engl.*, 1996, **35**, 1710.
27 D. Braga, F. Grepioni and A. G. Orpen, *Organometallics*, 1993, **12**, 1481.
28 T. L. Utz, P. A. Leach, S. J. Geib and N. J. Cooper, *Chem. Commun.*, 1997, 847.
29 J.-M. Bassett, D. E. Berry, G. K. Barker, M. Green, J. A. K. Howard and F. G. A. Stone, *J. Chem. Soc.*, *Dalton Trans.*, 1979, 1003.
30 P. Zolliker, K. Yon, P. Fischer and J. Schefer, *Inorg. Chem.*, 1985, **24**, 4177.
31 Y. S. Ng, G. A. Rodley and W. T. Robinson, *Inorg. Chem.*, 1976, **15**, 303.
32 E. F. Riedel and R. A. Jacobson, *Inorg. Chim. Acta*, 1970, **4**, 407.
33 F. A. Jurnak and K. A. Raymond, *Inorg. Chem.*, 1974, **13**, 2387.
34 K. N. Raymond, P. W. R. Corfield and J. A. Ibers, *Inorg. Chem.*, 1968, **7**, 1362.
35 M. Fritz, D. Rieger, E. Bar, G. Beck, J. Fuchs, G. Holzmann and W. P. Fehlhammer, *Inorg. Chim. Acta*, 1992, **198**, 513.
36 E. D. Estes and D. J. Hodgson, *Inorg. Chem.*, 1973, **12**, 2932.
37 J. H. Nelson and N. W. Alcock, *Inorg. Chem.*, 1982, **21**, 1196.
38 I. Bertini, P. Dapporto, D. Gatteschi and A. Scozzafava, *Inorg. Chem.*, 1975, **14**, 1639.
39 F. A. Jurnak, D. R. Greig and K. N. Raymond, *Inorg. Chem.*, 1975, **14**, 2585.
40 L. D. Brown, D. R. Greig and K. N. Raymond, *Inorg. Chem.*, 1975, **14**, 645.
41 L. D. Brown and K. N. Raymond, *Inorg. Chem.*, 1975, **14**, 2590.
42 D. Ramprasad, G. P. Pez, B. H. Toby, T. J. Markley and R. M. Pearlstein, *J. Am. Chem. Soc.*, 1995, **117**, 10694.
43 F. A. Cotton, T. G. Dunne and J. S. Wood, *Inorg. Chem.*, 1965, **4**, 318.
44 G. Albertin, E. Bordignon, A. Orio, G. Pelizzi and P. Tarasconi, *Inorg. Chem.*, 1981, **20**, 2862.
45 M. P. García, L. A. Oro and F. J. Lahoz, *Angew. Chem.*, *Int. Ed. Engl.*, 1988, **27**, 1700.
46 B. D. James, J. Liesegang, M. Bakalova, W. M. Reiff, B. W. Skelton and A. H. White, *Inorg. Chem.*, 1995, **34**, 2054.
47 M. Feist, S. I. Troyano, H. Mehner, K. Witke and E. Kemnitz, *Z. Anorg. Allg. Chem.*, 1999, **625**, 141.
48 G. A. Barclay, R. S. Vagg and E. C. Watton, *Acta Crystallogr.*, *Sect. B*, 1977, **33**, 3777.
49 K.-D. Scherfise, W. Willing, U. Muller and K. Dehnicke, *Z. Anorg. Allg. Chem.*, 1986, **534**, 85.
50 S. Kleinhenz and K. Seppelt, *Chem. Eur. J.*, 1999, **5**, 3573.
51 T. W. Coffindaffer, B. D. Steffy, I. P. Rothwell, K. Folting, J. C. Huffman and W. E. Streib, *J. Am. Chem. Soc.*, 1989, **111**, 4742.
52 C. J. Piersol, R. D. Profilet, P. E. Fanwick and I. P. Rothwell, *Polyhedron*, 1993, **12**, 1779.
53 T. J. Boyle, D. C. Bradley, M. J. Hampden-Smith, A. Patel and J. W. Ziller, *Inorg. Chem.*, 1995, **34**, 5893.
54 D. T. Corwin, Jr., J. F. Corning, S. A. Koch and M. Millar, *Inorg. Chim. Acta*, 1995, **229**, 335.
55 D. L. Clark, G. B. Deacon, T. Feng, R. V. Hollis, B. L. Scott, B. W. Skelton, J. G. Watkin and A. H. White, *Chem. Commun.*, 1996, 1729.
56 R. Gerardin, A. Alebongeh, F. Jeannot, A. Courtois, B. Malaman and O. Evrard, *Mater. Res. Bull.*, 1980, **15**, 647.
57 A. Rösler and D. Reinen, *Z. Anorg. Allg. Chem.*, 1981, **479**, 119.
58 P. C. Burns and F. C. Hawthorne, *Can. Miner.*, 1995, **33**, 885.
59 F. Beech, S. Miraglia, A. Santoro and R. S. Roth, *Phys. Rev. B*, 1987, **35**, 8778.
60 M. F. Garbauskas, R. W. Green, R. H. Arendt and J. S. Kaspert, *Inorg. Chem.*, 1988, **27**, 871.
61 C. C. Torardi, M. A. Subramanian, J. C. Calabrese, J. Gopalakrishnan, K. J. Morrissey, T. R. Askew, R. B. Flippen, U. Chowdhry and A. W. Sleight, *Science*, 1988, **240**, 631.
62 D. M. Proserpio, G. Chacon and C. Zheng, *Chem. Mater.*, 1998, **10**, 1286.
63 O. Ya. Mruz, V. K. Pecharsky, A. N. Solboev and O. I. Bodak, *Kristallogr.*, 1990, **35**, 202.
64 K. R. Poeppelmeier, M. E. Leonowicz and J. M. Longo, *J. Solid State Chem.*, 1982, **44**, 89.
65 J. P. Besse, G. Baud, G. Levasseur and P. Chevalier, *Acta Crystallogr.*, *Sect. B*, 1979, **35**, 1756.
66 P. J. Wheatley, *J. Chem. Soc.*, 1964, 2206.
67 C. P. Brock and D. F. Webster, *Acta Crystallogr.*, *Sect. B*, 1976, **32**, 2089.
68 A. L. Beauchamp, M. J. Bennett and F. A. Cotton, *J. Am. Chem. Soc.*, 1968, **90**, 6675.
69 C. Brabant, B. Blanck and A. L. Beauchamp, *J. Organomet. Chem.*, 1975, **82**, 231.
70 S. Wallenhauer, D. Leopold and K. Seppelt, *Inorg. Chem.*, 1993, **32**, 3948.
71 A. Schmuck, J. Buschmann, J. Fuchs and K. Seppelt, *Angew. Chem.*, *Int. Ed. Engl.*, 1987, **26**, 1180.
72 K. Nakamoto, *Infrared and Raman Spectra of Inorganic and Coordination Compounds*, 4th edition, J. Wiley and Sons, New York, 1986.
73 E. W. Ainscough, A. G. Bingham, A. M. Brodie, W. R. Ellis, H. B. Gray, T. M. Loehr, J. E. Plowman, G. E. Norris and E. N. Baker, *Biochemistry*, 1987, **26**, 71.
74 E. N. Baker, *J. Mol. Biol.*, 1988, **203**, 1071.
75 R. S. Berry, *J. Chem. Phys.*, 1960, **32**, 933.
76 E. L. Muetterties and L. J. Guggenberger, *J. Am. Chem. Soc.*, 1974, **96**, 1748.
77 H. B. Bürgi, *Acta Crystallogr.*, *Sect. A*, 1998, **54**, 873.
78 D. L. Kepert, *Inorganic Stereochemistry*, Springer-Verlag, Berlin, 1982.
79 J. K. Burdett, *Molecular Shapes. Theoretical Models of Inorganic Stereochemistry*, J. Wiley, New York, 1980.
80 D. W. Meek and J. A. Ibers, *Inorg. Chem.*, 1970, **9**, 465.
81 F. Fabrizi de Biani, E. Ruiz, J. Cano, P. Alemany and S. Alvarez, *Inorg. Chem.*, 2000, **39**, 3221.

82 H. Effenberger, *Monatsh. Chem.*, 1985, **116**, 927.
83 T. R. Ward, H.-B. Bürgi, F. Gilardoni and J. Weber, *J. Am. Chem. Soc.*, 1997, **119**, 11974.
84 H.-B. Bürgi, *Inorg. Chem.*, 1973, **12**, 2321.
85 D. Britton and J. D. Dunitz, *J. Am. Chem. Soc.*, 1981, **103**, 2971.
86 L. E. Khoo, N. K. Goh, G. Eng, D. J. Whalen and A. Hazell, *Appl. Organomet. Chem.*, 1995, **9**, 699.
87 W. N. Seik, *Main Group Met. Chem.*, 1995, **18**, 603.
88 S. Dondi, M. Nardelli, C. Pelizzi, G. Pelizzi and G. Predieri, *J. Organomet. Chem.*, 1986, **308**, 195.
89 K. C. Molloy, T. G. Purcell, K. Quill and I. W. Nowell, *J. Organomet. Chem.*, 1984, **267**, 237.
90 G. P. Voutsas, *Z. Kristallogr.-New Cryst. Struct.*, 1999, **214**, 31.
91 M. J. Cox and E. R. T. Tiekink, *Z. Kristallogr.-New Cryst. Struct.*, 1999, **214**, 49.
92 C. Pelizzi, G. Pelizzi and P. A. Tarasconi, *J. Organomet. Chem.*, 1977, **124**, 151.
93 W. N. Seik, *Acta Crystallogr.*, *Sect. C*, 1998, **54**, 1386.
94 R. Boese, B. Wrackmeyer and K. Wagner, Reported as a private communication to the Cambridge Structural Database, 1996.
95 G. Murphy, C. O'Sullivan, B. Murphy and B. Hathaway, *Inorg. Chem.*, 1998, **37**, 240 and references therein.
96 T. Kitagawa, M. Kita, K. Kashiwarbara and J. Fujita, *Bull. Chem. Soc. Jpn.*, 1991, **64**, 2942.
97 R. Bartsch, S. Hietkamp, S. Morton, H. Peters and O. Stelzer, *Inorg. Chem.*, 1983, **22**, 3624.
98 D. J. Brauer, F. Gol, S. Hietkamp, H. Peters, H. Sommer, O. Stelzer and W. S. Sheldrick, *Chem. Ber.*, 1986, **119**, 349.
99 B. J. Hathaway and A. Murphy, *Acta Crystallogr.*, *Sect. B*, 1980, **36**, 295.
100 M. A. Khan and D. G. Tuck, *Acta Crystallogr.*, *Sect. B*, 1981, **37**, 1409.
101 P. J. Burke, K. Henrick and D. R. McMillin, *Inorg. Chem.*, 1982, **21**, 1881.
102 J. Sletten and A. Sorensen, *Acta Chem. Scand.*, 1990, **44**, 1018.
103 R. P. Hammond, M. Cavaluzzi, R. C. Haushalter and J. A. Zubieta, *Inorg. Chem.*, 1999, **38**, 1288.
104 G. A. Barclay, B. F. Hoskins and C. H. L. Kennard, *J. Chem. Soc.*, 1963, 5691.
105 P. Nagle and B. J. Hathaway, *Acta Crystallogr.*, *Sect. C*, 1991, **47**, 1386.
106 T. W. Hambley, C. L. Raston and A. H. White, *Aust. J. Chem.*, 1977, **30**, 1965.
107 X.-L. Luo, G. J. Kubas, C. J. Burns, R. J. Butcher and J. C. Bryan, *Inorg. Chem.*, 1995, **34**, 6538.
108 W. A. King, B. L. Scott, J. Eckert and G. J. Kubas, *Inorg. Chem.*, 1999, **38**, 1069.
109 W. S. Sheldrick, *Z. Naturforsch.*, *Teil B*, 1983, **38**, 982.
110 S. Keinan and D. Avnir, *Inorg. Chem.*, submitted for publication.
111 W. D. Jones and E. Libertini, *Inorg. Chem.*, 1986, **25**, 1794.
112 Y. Fu, J. Sun, Q. Li, Y. Chen, W. Dai, D. Wang, T. C. W. Mak, W. Tang and H. Hu, *J. Chem. Soc.*, *Dalton Trans.*, 1996, 2309.
113 X.-Y. Liu and S. Alvarez, *Inorg. Chem.*, 1997, **36**, 1055 and references therein.
114 V. S. Mastryukov and S. H. Simonsen, *Adv. Mol. Struct. Res.*, 1996, **2**, 163.
115 C. A. Ghilardi, S. Midollini, A. Orlandini and A. Vacca, *J. Organomet. Chem.*, 1994, **471**, 29.
116 K. Kato and E. Takayama, *Acta Crystallogr.*, 1984, **40**, 102.
117 H. T. Evans, *Z. Kristallogr.*, 1960, **114**, 257.
118 A. Bjoernberg and B. Hedman, *Acta Chem. Scand.*, *Ser. A*, 1977, **31**, 579.
119 M. Bouwkamp, D. van Leusen, A. Meetsma and B. Hessen, *Organometallics*, 1998, **17**, 3645.
120 P. Y. Zavalij and M. S. Whittingham, *Acta Crystallogr.*, *Sect. B*, 1999, **55**, 627.
121 E. M. Page and S. A. Wass, in *Encyclopedia of Inorganic Chemistry*, vol. 8, ed. R. B. King, J. Wiley, New York, 1994, p. 4317.
122 C. R. Cornman, K. M. Geiser-Bush, S. P. Rowley and P. D. Boyle, *Inorg. Chem.*, 1997, **36**, 6401.
123 H. Sakurai, K. Fujii, S. Fujimoto, Y. Fujisawa, K. Takechi and H. Yasui, in *Vanadium Compounds. Chemistry*, *Biochemistry and Therapeutic Applications*, ed. A. S. Tracey and D. C. Crans, American Chemical Society, Washington, DC, 1998, p. 344.
124 K. H. Thompson, V. G. Yuen, J. H. McNeill and C. Orvig, in *Vanadium Compounds. Chemistry*, *Biochemistry and Therapeutic Applications*, ed. A. S. Tracey and D. C. Crans, American Chemical Society, Washington, DC, 1998, p. 329.
125 W. Priebsch and D. Rehder, *Inorg. Chem.*, 1990, **9**, 3013.
126 P. Caravan, L. Gelmini, N. Glover, F. G. Herring, H. Li, J. H. McNeill, S. J. Rettig, I. A. Setyawati, E. Shuter, Y. Sun, A. S. Tracey, V. G. Yuen and C. Orvig, *J. Am. Chem. Soc.*, 1995, **117**, 12759.
127 B. L. Westcott and J. H. Enemark, in *Inorganic Electronic Structure and Spectroscopy*, vol. 2, ed. E. I. Solomon and A. B. P. Lever, J. Wiley, New York, 1999, p. 403.
128 G. B. Richter-Addo and P. Legzdins, *Metal Nitrosyls*, Oxford University Press, New York, 1992.
129 J. H. Enemark and R. D. Feltham, *Coord. Chem. Rev.*, 1974, **13**, 339.
130 M. Ogasawara, D. Huang, W. E. Streib, J. C. Huffman, N. Gallego-Planas, F. Maseras, O. Eisenstein and K. G. Caulton, *J. Am. Chem. Soc.*, 1997, **119**, 8642.
131 F. H. Allen and O. Kennard, *Chem. Des. Automat. News*, 1993, **8**, 31.
132 D. Reinen and M. Atanasov, *Chem. Phys.*, 1989, **136**, 27.